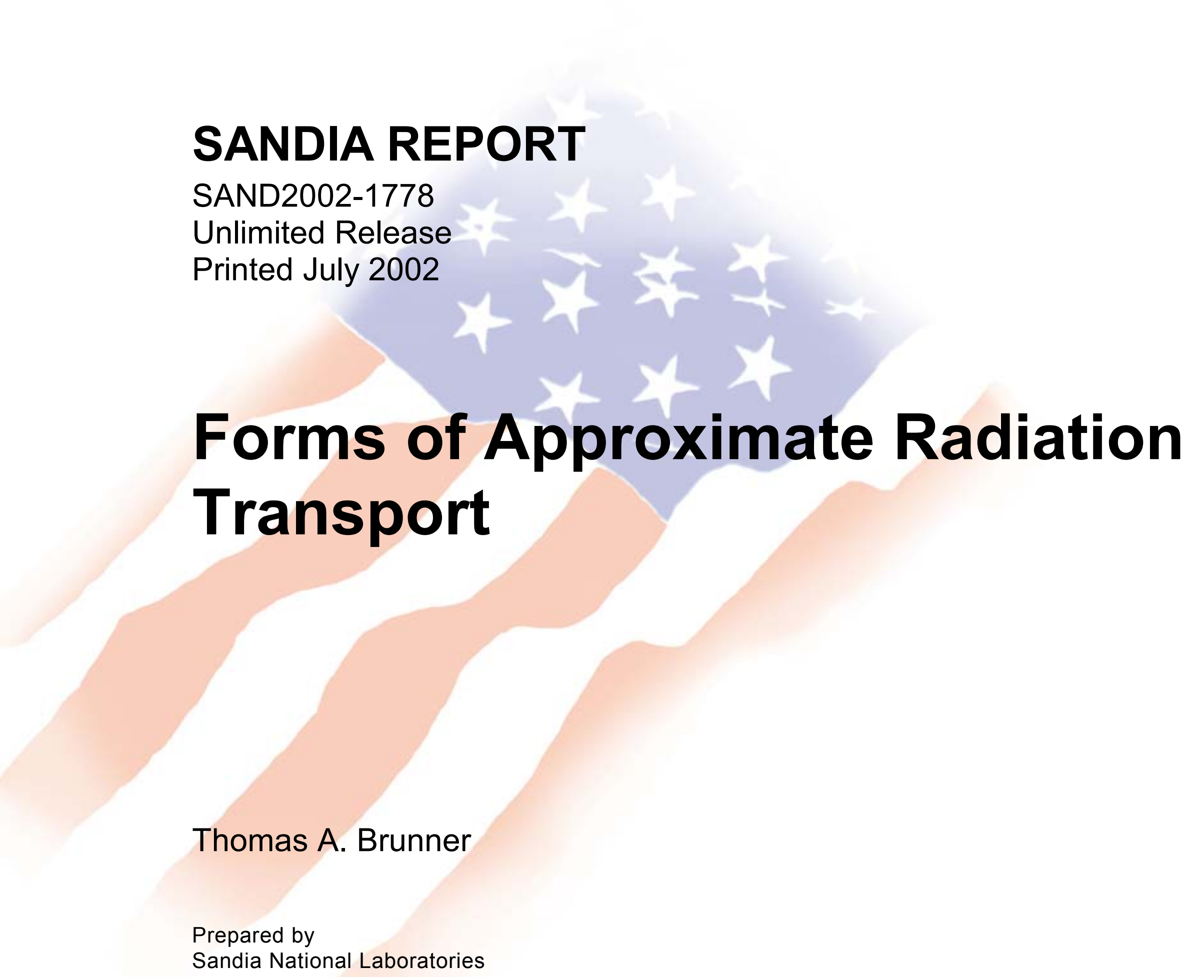

SANDIA REPORT

SAND2002-1778
Unlimited Release
Printed July 2002

Forms of Approximate Radiation Transport

Thomas A. Brunner

Prepared by
Sandia National Laboratories
Albuquerque, New Mexico 87185 and Livermore, California 94550

Sandia is a multiprogram laboratory operated by Sandia Corporation,
a Lockheed Martin Company, for the United States Department of
Energy under Contract DE-AC04-94AL85000.

Approved for public release; further dissemination unlimited.

Sandia National Laboratories

Issued by Sandia National Laboratories, operated for the United States Department of Energy by Sandia Corporation.

NOTICE: This report was prepared as an account of work sponsored by an agency of the United States Government. Neither the United States Government, nor any agency thereof, nor any of their employees, nor any of their contractors, subcontractors, or their employees, make any warranty, express or implied, or assume any legal liability or responsibility for the accuracy, completeness, or usefulness of any information, apparatus, product, or process disclosed, or represent that its use would not infringe privately owned rights. Reference herein to any specific commercial product, process, or service by trade name, trademark, manufacturer, or otherwise, does not necessarily constitute or imply its endorsement, recommendation, or favoring by the United States Government, any agency thereof, or any of their contractors or subcontractors. The views and opinions expressed herein do not necessarily state or reflect those of the United States Government, any agency thereof, or any of their contractors.

Printed in the United States of America. This report has been reproduced directly from the best available copy.

Available to DOE and DOE contractors from
U.S. Department of Energy
Office of Scientific and Technical Information
P.O. Box 62
Oak Ridge, TN 37831

Telephone: (865)576-8401
Facsimile: (865)576-5728
E-Mail: reports@adonis.osti.gov
Online ordering: http://www.doe.gov/bridge

Available to the public from
U.S. Department of Commerce
National Technical Information Service
5285 Port Royal Rd
Springfield, VA 22161

Telephone: (800)553-6847
Facsimile: (703)605-6900
E-Mail: orders@ntis.fedworld.gov
Online order: http://www.ntis.gov/ordering.htm

SAND2002-1778
Unlimited Release
Printed July 2002

Forms of Approximate Radiation Transport

Thomas A. Brunner
Target and Z-Pinch Theory
Sandia National Laboratories
P. O. Box 5800
Albuquerque, NM 87185-1186

Abstract

Photon radiation transport is described by the Boltzmann equation. Because this equation is difficult to solve, many different approximate forms have been implemented in computer codes. Several of the most common approximations are reviewed, and test problems illustrate the characteristics of each of the approximations. This document is designed as a tutorial so that code users can make an educated choice about which form of approximate radiation transport to use for their particular simulation.

Contents

1 The Transport Equation **9**
1.1 Radiation Transport 9

2 The Approximations **11**
2.1 Diffusion 12
2.1.1 The P_1 and Diffusion Approximations 13
2.1.2 Flux Limited Diffusion and Variable Eddington Factors 13
2.2 Discrete Ordinates 14
2.3 Spherical Harmonics 15
2.4 Monte Carlo 17

3 Multigroup Methods **18**

4 A Few Test Problems **20**
4.1 A Line Source in Two Dimensions 21
4.2 A Lattice Problem 23
4.3 A Hohlraum 27

5 Conclusions **32**

A Boundary Conditions **37**

B Physical Constants **39**

C Coordinate Systems **40**

Figures

1 Detailed aluminum opacity at 40 eV. 20
2 Solutions to the pulsed line source problem 22
3 The lattice problem schematic 24
4 The calculated energy density in the lattice problem at 3.2 seconds . . 25
5 The calculated energy density in the lattice problem at steady state . 26
6 The hohlraum problem schematic 27
7 The radiation temperature in the hohlraum problem early in time . . 29
8 The radiation temperature in the hohlraum problem late in time . . . 30
9 The material temperature in the hohlraum problem late in time . . . 31

Tables

1 The number of unknowns for discrete ordinates versus order 15
2 The number of unknowns for spherical harmonics versus order . . . 16
3 Coefficients for the diffusion boundary conditions. 39
4 Physical constants used in radiation transport 39

1 The Transport Equation

The Boltzmann transport equation describes how a variety of different types of particles travel through a material. It is generally considered the most accurate description of the statistical average density of particles in a system, as long as the particles do not interact with themselves.[1] A very general form of the Boltzmann transport equation is

$$\frac{1}{v}\frac{\partial f}{\partial t} + \mathbf{\Omega} \cdot \nabla f = \mathbf{C}(f), \tag{1}$$

where $f(\mathbf{x}, \mathbf{\Omega}, \varepsilon, t)$ is a phase space density with units of "things" per volume per energy per steradian, ε is the energy of the particles, $\mathbf{\Omega}$ is the direction of the particle travel, t is time, and $\mathbf{C}$ is a collision operator that represents all interactions with the material. The distribution function, f, is seven dimensional: three space, two angle, one energy, and one time dimension. The first term of Eq. 1 is the rate of change in f with respect to time; all the other terms tally what processes cause the distribution f to change. The second term is called the streaming term; it describes the rate of change in f at a point because the particles are moving. All of the physics that describes how particles, such as photons or neutrons, interaction with the material is contained in the collision operator.

Eq. 1 is difficult to solve directly, and approximation is nearly always made before solving it. This paper reviews several of the most popular approximations used in the radiation transport community.

1.1 Radiation Transport

The Boltzmann equation, Eq. 1, is very general, and every discipline has a different way to write it that fits their needs best. In radiation transport, the photon density is not as important as the energy density of the photons. Instead of solving for f, the radiation community solves for $I(\mathbf{r}, \mathbf{\Omega}, \varepsilon, t) = h\nu f$, where ν is the photon frequency with energy $\varepsilon = h\nu$, h is Planck's constant, I is called the intensity[2] and roughly describes the radiation energy density flowing in a particular direction. Multiplying Eq. 1 by $h\nu$ and expanding the collision operator $\mathbf{C}$ gives us an equation for the intensity, namely

$$\frac{1}{c}\frac{\partial I}{\partial t} + \mathbf{\Omega} \cdot \nabla I = -\sigma_t I + \frac{\sigma_s}{4\pi}\int_{4\pi} I \ \mathrm{d}\mathbf{\Omega}' + \sigma_a B(T_m, \varepsilon) + S \tag{2}$$

In addition to Eq. 2, which describes the energy density of the photons, there is another equation that describes the energy content of the material. This equation is

$$\frac{\partial u_m}{\partial t} = -\int_0^\infty \int_{4\pi} c\sigma_a (B(T_m, \varepsilon) - I) \ \mathrm{d}\mathbf{\Omega} \ \mathrm{d}\varepsilon, + Q_m \tag{3}$$

---

[1] It will not work to describe the gas in a balloon, for example.

[2] The intensity is often defined as $I = ch\nu f$, which describes the power flowing through particular surface in a particular direction.

where c is the speed of light, $\mathbf{\Omega}$ is the unit angle vector, u_m is the material energy density, $T_m(u_m)$ is the material temperature and is a function of the material energy, $\sigma_t = \sigma_s + \sigma_a$ are the total, scattering, and absorption opacities with units of inverse length and are also functions of the material energy, S is an external source of photon energy, Q_m is an external source of material heating, and $B(T_m, \varepsilon)$ is Planck's function.

Eq. 2 assumes local thermal equilibrium and that that the scattering is isotropic and elastic; there are many instances where these are not valid assumptions, and more complicated scattering terms must be used. The left hand side of Eq. 3 describe the imbalance between the radiation intensity and the material energy. The primary difficulties in numerically solving all forms of radiation transport are caused by this term; the intensity I and Planck's function generally have extremely large values, but their difference is quite small.

The intensity I contains much more detailed information than is frequently needed to solve a particular problem. In fact, the coupling with the material in Eq. 3 is only through the integral of I over all energies and angles. Integrating I over all angles yields

$$E = \int_{4\pi} I \, \mathrm{d}\mathbf{\Omega} \,, \tag{4}$$

where E is the monochromatic, or energy dependent, radiation energy density[3] The radiation energy density is one of the primitive variables in a several of the approximations to Eq. 2.

When the radiation field is in equilibrium with the material, the Planck (or black body) function describes the intensity I as a function of energy; this function is

$$B(T_m, \varepsilon) = \frac{2}{h^3 c^3} \frac{\varepsilon^3}{\left(\mathrm{e}^{\varepsilon/kT_m} - 1\right)}, \tag{5}$$

where k is the Boltzmann constant and is the proportionality constant between temperature and energy. The maximum in the Planck function is at a photon energy of

$$\varepsilon_{\text{max}} = (2.82143937212207889 34 ...)kT. \tag{6}$$

When the material and radiation are not in equilibrium, the material emits radiation with a power density of $c\sigma_a B$ and the photons are absorbed with a power density of $c\sigma_a I$. Integrating the Planck function B over all energies and angles as in Eq. 3 yields

$$B_E(T_m) = \frac{8\pi^5 k^4}{15 h^3 c^3} T_m^4 = a T_m^4, \tag{7}$$

where a is the black body constant. Just as the material at a given temperature has a known radiation field, the radiation can be characterized in terms of a temperature using

---

[3] Within the radiation transport community, there are several groups, each of which used their own notation. Astrophysicists tend to use the mean intensity $J = cE/4\pi$, while others use E. E will be used here.

$$T_r = \left(\frac{1}{a} \int_0^\infty E \, \mathrm{d}\varepsilon \right)^{\frac{1}{4}} . \tag{8}$$

Equations 2 and 3 form a nonlinear system, even if the material properties are constant. They can be quite difficult to solve, even when Eq. 2 is approximated. Many people have looked at how to deal with the nonlinearity [8, 9, 26, 18]. There are also some excellent general references on radiation transport [33, 39, 29, 16, 2].

2 The Approximations

There are several main approximations to Eq. 2 that most people use. They are:

1. Diffusion [15, 12, 14, 11, 9, 43, 25, 38, 6, 5, 31, 35, 44, 46, 27, 37, 1, 42, 41, 28]
    (a) Flux Limited Diffusion
    (b) Variable Eddington Factors
2. Discrete Ordinates (S_N) [4, 32, 2, 40, 34, 39, 2, 47]
3. Spherical Harmonics (P_N) [7, 10, 40, 13]
4. Implicit Monte Carlo (IMC) [17, 22]

The diffusion equation is very easy to solve but is inaccurate in optically thin regions and where the gradient of the energy density is large. Flux limited diffusion is an improvement to fix these deficiencies at the cost of making the equations nonlinear. Diffusion and P_1 are very closely related; variable Eddington factor approximations are a nonlinear improvement upon the P_1 approximation, much in the same way that flux limited diffusion improves upon regular diffusion.

The equations that arise in the discrete ordinates (S_N) approximation are also very easy to solve, especially in serial calculations. Recent work has gone into making S_N work on unstructured meshes in parallel. The most severe problem that S_N has is the inclusion of artifacts in the solution called ray effects.

The spherical harmonics approximation (P_N) has been around for a long time, but has not gotten much use in large codes. While S_N suffers from ray effects, P_N suffers from wave effects in time dependent problems

Monte Carlo is not an approximation of the transport equation. While the transport equation describes the statistical average of the particles in the system, Monte Carlo methods try to build up an average by simulating many individual particles. Because it is infeasible to simulate as many particles as there are in the physical system, the accuracy of the solution is usually limited by computer time and memory.

Only the Boltzmann equation, Eq. 2, is being approximated in all these methods; the material energy equation, Eq. 3, is unchanged.

2.1 Diffusion

Because the various forms of diffusion are so common, it is important to understand how it is derived from the transport equation (Eq. 2). The derivation will also show how diffusion, flux limited diffusion, and variable Eddington factor methods are related.

For many problems, only the energy density E is important. In fact, it is this quantity that shows up in Eq. 3. Instead of solving for I directly and then integrating over angle to compute E indirectly, we can manipulate Eq. 2 to yield an equation for E instead of I. The first step is to integrate Eq. 2 over angle to yield

$$\frac{1}{c}\frac{\partial E}{\partial t} + \nabla \cdot \mathbf{F} = \sigma_a(4\pi B(T_m) - E) + S_E, \tag{9}$$

where

$$\mathbf{F} = \int_{4\pi} \mathbf{\Omega} I \, \mathrm{d}\mathbf{\Omega}\,, \tag{10}$$

is the radiative flux and is the first angular moment of I[4], S_E is a source of radiation energy density, and we have used the fact that $\sigma_a = \sigma_t - \sigma_s$[5] Unfortunately, we now have a new unknown, $\mathbf{F}$. To get an equation for $\mathbf{F}$ as well, we can "easily" take the first moment of Eq. 2 yielding

$$\frac{1}{c}\frac{\partial \mathbf{F}}{\partial t} + \nabla \cdot \boldsymbol{\chi} E = -\sigma_t \mathbf{F}, \tag{11}$$

where it has been assumed that all sources of particles (the external source, $B(T_m)$, and scattering) are isotropic, and $\boldsymbol{\chi}$ is the Eddington tensor,

$$\boldsymbol{\chi} = \frac{1}{E}\int_{4\pi} (\mathbf{\Omega} \otimes \mathbf{\Omega})\, I \, \mathrm{d}\mathbf{\Omega}\,, \tag{12}$$

where the symbol "$\otimes$" signifies an outer product.[6] The Eddington factor $\boldsymbol{\chi}$ is the normalized radiation pressure.

This first moment equation is coupled to the second moment. We could keep taking higher and higher moments of Eq. 2, but each equation is always coupled to the next higher moment. In fact the P_N approximation essentially comes from this procedure. (See Section 2.3.) All diffusion-like approximations make some approximation for $\boldsymbol{\chi}$ in order to close the equations.

---

[4] Again, a different normalization is commonly used for the flux such that $\hat{\mathbf{F}} = c\mathbf{F}$ which has units of power per area.

[5] $\sigma_t = \sigma_s + \sigma_a$ is only valid for the energy dependent equations; once the energy is discretized and averages created for each of these quantities, this relation might not be true.

[6] An outer product operates on two vectors to yield a tensor. This is "opposite" of an inner product that computes a scalar from two vectors.

2.1.1 The P_1 and Diffusion Approximations

The most common approximation is to assume that the radiation intensity, I, varies linearly with angle,

$$I(\mathbf{r}, \mathbf{\Omega}, t) = \frac{1}{4\pi}E + \frac{3}{4\pi}\mathbf{\Omega} \cdot \mathbf{F}. \tag{13}$$

The approximation that the distribution is nearly isotropic is good in systems that are optically thick. With this approximation, Eq. 12 becomes simply

$$\boldsymbol{\chi} = \frac{1}{3}\mathbf{I}, \tag{14}$$

where $\mathbf{I}$ is the identity tensor. With this, Eq. 9 and Eq. 11 become the system of equations

$$\frac{1}{c}\frac{\partial E}{\partial t} + \nabla \cdot \mathbf{F} = \sigma_a(4\pi B(T_m) - E) + S_E \tag{15}$$

$$\frac{1}{c}\frac{\partial \mathbf{F}}{\partial t} + \frac{1}{3}\nabla E = -\sigma_t \mathbf{F} \tag{16}$$

This is the P_1 approximation. One further approximation can be made, namely that the flux $\mathbf{F}$ varies slowly with time in comparison to the spatial gradient,

$$\frac{1}{c}\frac{\partial \mathbf{F}}{\partial t} \ll \frac{1}{3}\nabla E \tag{17}$$

This implies Fick's law $\mathbf{F} = -1/3\sigma_t \nabla E$ and leads to the diffusion approximation. This has the advantage of only one equation to solve for the energy density E. The diffusion equation and the material equation are

$$\frac{1}{c}\frac{\partial E}{\partial t} - \nabla \cdot D\nabla E = \sigma_a \left(4\pi B(T_m) - E\right) + S_E. \tag{18}$$

$$\frac{\partial u_m}{\partial t} = \int_0^\infty c\sigma_a \left(E - 4\pi B(T_m)\right) \, \mathrm{d}\varepsilon + Q_m, \tag{19}$$

where $D = 1/3\sigma_t$ is the diffusion coefficient.

There has been a fundamental change in the form of the equations; the transport equation (Eq. 2) is hyperbolic, implying that particles (and energy) travels at finite speeds. Ignoring the time derivative in Eq. 16 makes the resulting time dependent diffusion equation parabolic, allowing the particles to travel at infinite speed; a small change in one part of the problem immediately affects every other part of the problem.

2.1.2 Flux Limited Diffusion and Variable Eddington Factors

A large source of problems with both the P_1 and diffusion approximations comes from the fact that they allow $|\boldsymbol{\eta}| > 1$, where

$$\boldsymbol{\eta} \equiv \frac{\mathbf{F}}{Er}. \tag{20}$$

This is completely unphysical; it implies that more energy can be moving than exists at a point to begin with, or, in other words, the flux $\mathbf{F}$ is not limited by the energy density. To correct this problem, other approximations of the intensity I instead of the one in Eq. 13 are made where the flux $\mathbf{F}$ is limited; hence the name "Flux Limited Diffusion". The variable Eddington factor equations are the P_1 equations, Eq. 9 and Eq. 11, namely

$$\frac{1}{c}\frac{\partial E}{\partial t} + \nabla \cdot \mathbf{F} = \sigma_a(4\pi B(T_m) - E) + S_E \tag{21}$$

$$\frac{1}{c}\frac{\partial \mathbf{F}}{\partial t} + \nabla \boldsymbol{\chi} E = -\sigma_t \mathbf{F}, \tag{22}$$

where the Eddington tensor $\boldsymbol{\chi}$ is a nonlinear function of E. There are many different closures for $\boldsymbol{\chi}$ that have been proposed [38, 35, 31, 44, 25, 30].

The flux limited diffusion equations are arrived at by further assuming that Eddington factor $\boldsymbol{\chi}$ is "isotropic" ($\boldsymbol{\chi} = \chi\mathbf{I}$), that $\boldsymbol{\chi}$ varies slowly with space, and that the approximation in Eq. 17 holds. Using these approximations we can write down the flux limited diffusion equation as

$$\frac{1}{c}\frac{\partial E}{\partial t} - \nabla \cdot \frac{\chi}{\sigma_t}\nabla E = \sigma_a(4\pi B(T_m) - E) + S_E. \tag{23}$$

The material energy equation is still Eq. 19.

One commonly used flux limiter is the simplified Levermore-Pomraning flux limiter [31]. It sets

$$\chi = \frac{1}{R}\left[\coth R - \frac{1}{R}\right], \quad \text{where} \quad R = \frac{\nabla E}{\sigma_t E} \tag{24}$$

This is derived from an exact solution of the transport equation for a particular problem, and does remarkably well on a wide variety of problems. Other flux limited diffusion schemes are used [31, 44, 25], and they also do very well in practice. One approach uses a a higher order approximation such as S_N, P_N, or IMC every few steps which is then used to calculate a $\boldsymbol{\chi}$ for use in the variable Eddington factor and flux limited diffusion approximations.

Flux limited diffusion is nearly as cheap as regular diffusion to compute, and much, much cheaper than any of the higher order approximations. This accounts for its extraordinary popularity and usefulness for the foreseeable future.

2.2 Discrete Ordinates

The discrete ordinates approximation assumes that particles can only travel along a few particular directions, instead of the infinite number of directions allowed in Eq. 2. These directions are generally chosen to be symmetric for any ninety degree rotation of the coordinate system. Mathematically, this approximation assumes

	Quadrature Order				
Dimensions	2	4	8	16	N
One	2	4	8	16	N
Two	4	12	40	144	$\frac{1}{2}N^2 + N$
Three	8	24	80	288	$N^2 + 2N$

Table 1: The number unknowns versus quadrature order for the discrete ordinates, or S_N, approximation.

that the intensity is a sum of delta functions,

$$I(\mathbf{r}, \mathbf{\Omega}, \varepsilon, t) = \sum_{n=1}^{M} I_n(\mathbf{r}, \varepsilon, t)\delta(\mathbf{\Omega} - \mathbf{\Omega}_n). \tag{25}$$

If we insert this into Eq. 2, we find that we have N different equations, one for each direction (or ordinate) $\mathbf{\Omega}_n$,

$$\frac{1}{c}\frac{\partial I_n}{\partial t} + \mathbf{\Omega}_n \cdot \nabla I_n = -\sigma_t I_n + \frac{\sigma_s}{4\pi}\sum_{m=1}^{M} w_m I_m + \sigma_a B(T_m) + S_n, \tag{26}$$

where w_m is an integration weight. Each direction n is coupled to all the others through the scattering term and the material equation. Eq. 26 can be differenced in an upwinded manner, leading to a very efficient algorithm called transport sweeps. On unstructured grids, it is possible to get cycles of dependency,[7] and the sweep algorithm fails. These cycles can be detected and broken, allowing the sweeps to continue.

The discrete ordinates approximation in more than one spatial dimension has a well-known defect called ray effects [32, 34, 7]. Due to the discrete nature of the angular approximation, particles do not reach regions where they otherwise would, sometimes producing large spatial oscillations in the energy density E. There have been some attempts to eliminate ray effects by introducing extra terms into the equations that act like extra scattering [4, 40, 24].

The N in the abbreviation S_N comes from the quadrature order. In one dimension, the quadrature order is equal to the number of directions in Eq. 25. In two and three dimensions, the number of directions is much more. Table 1 lists the number of unknowns (or ordinates) for a few quadrature orders as well as expressions for arbitrary N.

2.3 Spherical Harmonics

The derivation of spherical harmonics approximation is very similar to the derivation of the diffusion approximation. In the diffusion approximation, we only took

---

[7] Imagine a ring of cells. Where is the beginning?

	Expansion Order				
Dimensions	1	3	7	15	N
One	2	4	8	16	$N+1$
Two	3	10	36	136	$\frac{1}{2}N^2+\frac{3}{2}N+1$
Three	6	20	72	272	N^2+3N+2

Table 2: The number unknowns versus expansion order for the spherical harmonics, or P_N, approximation.

the first two angular moments of the transport equation. In the spherical harmonics approximation, we can take as many moments as we need for an accurate solution. The intensity, I, is expanded with a set of orthonormal functions called the spherical harmonic functions,

$$I(\mathbf{r},\mathbf{\Omega},\varepsilon,t) = \frac{1}{\sqrt{4\pi}}\sum_{l=0}^{\infty}\sum_{m=-l}^{l} E_l^m(\mathbf{r},\varepsilon,t)Y_l^m(\mathbf{\Omega}) \tag{27}$$

$$E_l^m(\mathbf{r},\varepsilon,t) = \sqrt{4\pi}\int_{4\pi}\overline{Y}_l^m(\mathbf{\Omega})I(\mathbf{r},\mathbf{\Omega},\varepsilon,t)\,\mathrm{d}\mathbf{\Omega}\,, \tag{28}$$

where E_l^m is the moment of I with respect to the spherical harmonic function Y_l^m. The lowest order spherical harmonic $Y_0^0 = 1/\sqrt{4\pi}$, so the multiply and divide by $\sqrt{4\pi}$ in Eq. 27 and Eq. 28 is so that $E_0^0 = E$ is the energy density. The P_N approximation[8] arises when it is then assumed that if $l \geq N$, then moments $E_l^m = 0$.

If we multiply Eq. 2 by each $\overline{Y}_l^m$[9] and integrate over angle, we get a series of equations for the moments of the intensity I. Each moment E_l^m is only coupled to the moments $E_{l'}^{m'}$, where $l' = l \pm 1$ and $m' = m + \{-1, 0, 1\}$, for a total of six other moments. This system of equations can be written in vector form as

$$\frac{1}{c}\frac{\partial \mathbf{E}}{\partial t} + \mathbf{A}_x\frac{\partial \mathbf{E}}{\partial x} + \mathbf{A}_y\frac{\partial \mathbf{E}}{\partial y} + \mathbf{A}_z\frac{\partial \mathbf{E}}{\partial z} = -\sigma_t\mathbf{E} + \mathbf{S}, \tag{29}$$

where $\mathbf{A_i}$ are the Jacobians with respect to the $\mathbf{i}^{\text{th}}$ direction describing the details of how the moments are coupled, $\mathbf{E}$ is a vector of the moments E_l^m, and $\mathbf{S}$ is the source vector and contains the scattering and material emission terms. The Jacobians $\mathbf{A_i}$ are constant in space and share a remarkable property—the eigenvalues of each matrix are identical. Particles travel in waves through the system at a finite number of speeds determined by these eigenvalues. The more moments, the more eigenvalues, the more different speeds, and the more accurate the solution can be. Table 2 lists the number of unknowns in $\mathbf{E}$ for a few expansion orders. Comparing the figures in Table 1 and Table 2 shows that an S_N approximation has roughly the same degrees of freedom as a P_{N-1} approximation.

---

[8] The symbol P is used because it is the symbol for the Legendre polynomials. In one dimension, the spherical harmonic functions reduce to the Legendre polynomials.

[9] The complex conjugate of Y_l^m.

The spherical harmonics approximation has a not-so-well-known defect called wave effects in the time dependent case. In a vacuum, the system of equations is a wave equation, and it is possible to get negative energy densities $E = E_0^0$. This is clearly unphysical. Not only is this important for vacuum regions, but on short time scales, interactions with the material become unimportant, and the equations again look like they are in a vacuum. Even in time dependent problems without voids, it is possible to get a negative solution for the energy density E. The energy density in steady state problems is always nonnegative.

2.4 Monte Carlo

The Boltzmann transport equation (Eq. 2) and approximations based on it solve for the statistical average of energy densities. It treats the radiation as a continuous field; particles do not really exist.

Monte Carlo, on the other hand, embraces the particle as its fundamental feature. Individual photons are simulated from birth to death, modifying the material energy as they travel. When a simulated photon is emitted from the material, it slightly decreases the material energy. This photon travels through the model, occasionally interacting with the material through scattering or absorption events. When the photon is absorbed, the material energy is incremented a little bit.

All of the photon's interactions, including its birth, have certain probabilities of occurring that we can estimate. A pseudo random number generator is used in conjunction with these probabilities to calculate when, where, and what kind of event occurred. Once many particles have been simulated, a reasonable average for the energy density is estimated.

Implicit Monte Carlo, or IMC, is a particular way to handle the time dependence for radiation transport problems. In IMC, as the photons heat or cool the material during the time step, the probability that photons are emitted from the material change. Despite the name of the method, the material properties such as opacity and density are fully explicit; only the emission rate from the material is treated implicitly. At the end of each time step, the photon population is counted, and the material properties incremented.

The biggest disadvantage of IMC is that it is both processor time and memory intensive; otherwise, it generally yields very accurate results, once enough particles have been simulated. Until a photon dies in an IMC simulation, it remains in memory. For a three dimensional problem, energy dependent calculation, one million particles would use about 45 MB of memory.[10]

---

[10] This is an absolute minimum and assumes one double precision variable for each of the three position, two angle, and one energy variables. Other information such as the random number generator state, particle time, etc. can increase this number significantly.

The estimated error in the IMC calculation is

$$\text{Error} = \alpha \frac{1}{\sqrt{N}}, \tag{30}$$

where α is some proportionality constant and N is the number of particles simulated. This equation implies that in order to achieve a factor of 10 decrease in the estimated error, 100 times more particles need to be simulated! There are many variance reduction techniques that can be used to dramatically reduce the proportionality constant α, but the general scaling of error with the number particles simulated shown in Eq. 30 still applies.

In very rare instances, the simulation can produce a completely wrong result, especially if something important happens where there are not very many photons.[11] While deterministic approximations (diffusion, S_N, P_N) have a uniform error throughout the system, the Monte Carlo simulation has the largest error where there are the fewest particles. It has been argued that this is actually a good thing because Monte Carlo spends its time getting a good answer where it matters, if that is defined as the highest particle density. (This can be a reasonable assumption.) The deterministic approximations get equally good (or bad) results everywhere.

3 Multigroup Methods

The transport equation, Eq. 2, depends on photon energy. In order to form a problem that we can solve numerically, Eq. 2 (or any approximation based on it) is usually discretized in energy by integrating it over energy range to yield

$$\int_{\varepsilon^g_{\text{min}}}^{\varepsilon^g_{\text{max}}} \left[\frac{1}{c}\frac{\partial I}{\partial t} + \mathbf{\Omega} \cdot \nabla I = -\sigma_t I + \frac{\sigma_s}{4\pi} \int_{4\pi} I \; \mathrm{d}\mathbf{\Omega}' \; + \sigma_a B(T_m) + S \right] \mathrm{d}\varepsilon \tag{31}$$

This leads to a series of equations for each energy range called the group equations:

$$\frac{1}{c}\frac{\partial I_g}{\partial t} + \mathbf{\Omega} \cdot \nabla I_g = -\overline{\sigma}^g_t I_g + \frac{1}{4\pi} \int_{4\pi} \overline{\sigma}^g_s I_g \; \mathrm{d}\mathbf{\Omega}' \; + \overline{\sigma}^g_a B_g(T_m) + S_g, \tag{32}$$

where $I_g = \int_{\varepsilon^g_{\text{min}}}^{\varepsilon^g_{\text{max}}} I \, \mathrm{d}\varepsilon$ and similarly for S_g and B_g. Some of the terms in Eq. 32 are more complicated; however, careful averages can be performed to ensure that the terms are equal to the terms in Eq. 31. Inspecting the emission term first, we define an averaged opacity such that

$$\overline{\sigma}^g_a = \frac{\int_{\varepsilon^g_{\text{min}}}^{\varepsilon^g_{\text{max}}} \sigma_a(T_m, \varepsilon) B(T_m, \varepsilon) \, \mathrm{d}\varepsilon}{\int_{\varepsilon^g_{\text{min}}}^{\varepsilon^g_{\text{max}}} B(T_m, \varepsilon) \, \mathrm{d}\varepsilon}, \tag{33}$$

---

[11] Consider the case of a supercritical nuclear reactor behind a very thick neutron shield. Since pure uranium is not an emitter of neutrons, there is nothing to initiate run-away chain reaction in the reactor, except for the source of neutrons on the other side of the shield. A Monte Carlo simulation might not ever transport a neutron to the reactor, giving you a false sense of security. In the real world, there would be so many neutrons, the probability that at least one will reach the reactor is very great.

where $\overline{\sigma}_a^g$ is called the Planck weighted average. The emission term in Eq. 31 can be expressed exactly as $\overline{\sigma}_a^g B_g$, where $B_g = \int_{\varepsilon_{\text{min}}^g}^{\varepsilon_{\text{max}}^g} B \, \mathrm{d}\varepsilon$ is the group integrated Planck function. Ideally we would want to average the total removal and scattering terms in a similar fashion, using

$$\overline{\sigma} = \frac{\int_{\varepsilon_{\text{min}}^g}^{\varepsilon_{\text{max}}^g} \sigma(T_m, \varepsilon) I(\varepsilon) \, \mathrm{d}\varepsilon}{\int_{\varepsilon_{\text{min}}^g}^{\varepsilon_{\text{max}}^g} I(\varepsilon) \, \mathrm{d}\varepsilon} \tag{34}$$

to calculate the average. However we do not (and do not want to) know what the detailed energy density $I(\varepsilon)$. We are making the group approximation so that we don't have solve for this in the first place. If we assume that the simulation is nearly in equilibrium, then $I \approx B$, and we can just use a Planck average as in Eq. 33.

The diffusion equation Eq. 18 in Section 2.1.1 has an opacity that shows up in a slightly different form in the diffusion term. Integrating the diffusion term in Eq. 18 over a group yields

$$\int_{\varepsilon_{\text{min}}^g}^{\varepsilon_{\text{max}}^g} \nabla \cdot \frac{1}{3\sigma_t} \nabla E \, \mathrm{d}\varepsilon = \nabla \cdot \frac{1}{3} \int_{\varepsilon_{\text{min}}^g}^{\varepsilon_{\text{max}}^g} \frac{1}{\sigma_t} \nabla E \, \mathrm{d}\varepsilon. \tag{35}$$

This equation suggests a different average that looks like a harmonic mean. Again, since we do not know the energy density E, we can make the assumption that it is approximately equal to B. This gives us the Rosseland mean opacity, which is defined as

$$\frac{1}{\overline{\sigma}_R^g} = \frac{\int_{\varepsilon_{\text{min}}^g}^{\varepsilon_{\text{max}}^g} \frac{1}{\sigma_t} \nabla B \, \mathrm{d}\varepsilon}{\int_{\varepsilon_{\text{min}}^g}^{\varepsilon_{\text{max}}^g} \nabla B \, \mathrm{d}\varepsilon} = \frac{\int_{\varepsilon_{\text{min}}^g}^{\varepsilon_{\text{max}}^g} \frac{1}{\sigma_t} \frac{\partial B}{\partial T_m} \nabla T_m \, \mathrm{d}\varepsilon}{\int_{\varepsilon_{\text{min}}^g}^{\varepsilon_{\text{max}}^g} \frac{\partial B}{\partial T_m} \nabla T_m \, \mathrm{d}\varepsilon} = \frac{\int_{\varepsilon_{\text{min}}^g}^{\varepsilon_{\text{max}}^g} \frac{1}{\sigma_t} \frac{\partial B}{\partial T_m} \, \mathrm{d}\varepsilon}{\int_{\varepsilon_{\text{min}}^g}^{\varepsilon_{\text{max}}^g} \frac{\partial B}{\partial T_m} \, \mathrm{d}\varepsilon} \tag{36}$$

When the radiation community uses the term "Rosseland mean opacity", they are referring to precisely Eq. 36, which is the weighted harmonic mean of the total opacity. Also when the term "Planck mean opacity" is used, they are referring to the arithmetic weighted average of the absorption opacity in Eq. 33. Note that when using the Rosseland mean, $\overline{\sigma}_t^g \neq \overline{\sigma}_s^g + \overline{\sigma}_a^g$.

One could use either the Plank or Rosseland mean averages for any opacity that appears in the equations, and frequently a Rosseland mean is used on all opacities that arise. Figure 1 shows a detailed total opacity for aluminum at 40 eV and an ion density of $10^{19}\,\mathrm{cm}^{-3}$ calculated with a program written by Ping Wang [45]. Also shown on the figure is the one and five group average opacities calculated as a Planck mean and a Rosseland mean. The Rosseland mean, because is is essentially a harmonic mean, weights the lower opacities more. To see why using the Rosseland mean makes physical sense, imagine a slab of 40 eV aluminum with a source of radiation shining on it. A few mean free paths into the slab, most of the photons will have been absorbed, except for the ones with energies around

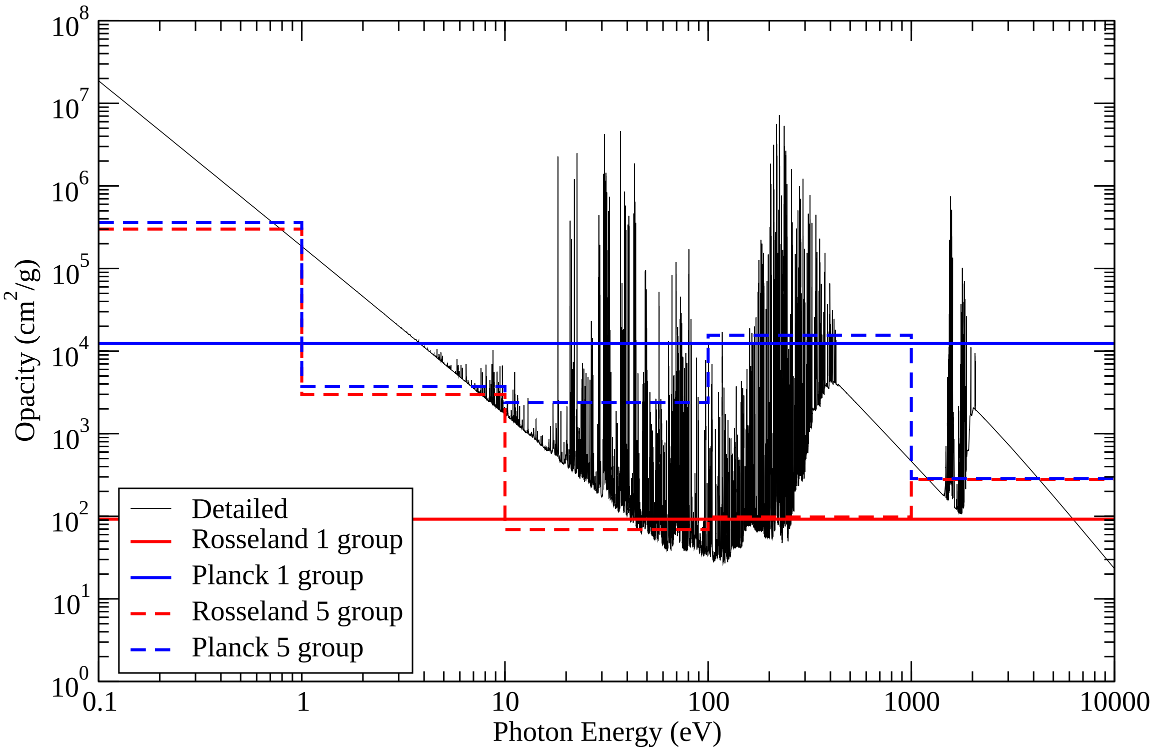

Figure 1: The detailed aluminum opacity at 40 eV and an ion density of $10^{19}\ \mathrm{cm}^{-3}$ is shown with one and five group Planck and Rosseland means. Note how the Rosseland mean is weighted toward the lower opacities.

100 eV (the minimum in the detailed opacity). If we were then to use the ideal averaging method in Eq. 34 to calculate an average opacity, it would be heavily weighted toward this minimum because the distribution of $I(\varepsilon)$ is peaked in that energy range. The harmonic mean qualities of the Rosseland mean automatically does this without needing the detailed distribution of $I(\varepsilon)$.

For many calculations a single energy group is detailed enough for an accurate answer. In this case, the integration in Eq. 32 is carried out over all energies. This one-group approximation is sometimes called the gray approximation.

4 A Few Test Problems

The problems in this section are designed to give some insight as to how the various approximation perform relative to each other. Some of the problems are a test of neutral particle transport; they are not coupled to the material energy at all. All of the calculations are single-group in energy.

4.1 A Line Source in Two Dimensions

The most basic of all time dependent problems is a Green's function problem. In two dimensions this is a pulse of particles is emitted from a line source. In a linear system such as ours without the material equation, solutions to all other time dependent problems are just superpositions of solutions of different Green's function problems. Only a vacuum is considered here; there is no coupling with the material. This test problem is designed to show the fundamental differences in each of the approximations. The defects in each of the approximations that are exposed by this problem will also be seen in all of the other test problems considered in later sections.

The energy density can be solved for analytically for most approximations. Solving the transport equation, Eq. 2, for the intensity I, then integrating over angle to get the energy density E yields

$$E^{\text{transport}} = \frac{E^0}{2\pi} \frac{\mathrm{h}(ct - r)}{ct\sqrt{c^2t^2 - r^2}}, \tag{37}$$

where E^0 is the strength of the initial radiation pulse along the line and $\mathrm{h}(x)$ is the unit step function. The general P_N solution is

$$E^{P_N} = \frac{E^0}{\pi} \sum_{\lambda_i \geq 0} r_i l_i \left[\frac{\delta(r - \lambda_i t)}{\sqrt{\lambda_i^2 t^2 - r^2}} - \frac{\lambda_i t\, \mathrm{h}(\lambda_i t - r)}{(\lambda_i^2 t^2 - r^2)^{3/2}} \right], \tag{38}$$

Note that there are regions where the solution for E^{P_N} is negative. This is an essential defect of the P_N equations, not a problem with the numerical implementation. The general S_N solution is

$$E^{S_N} = E^0 \sum_i w_i \delta(\|\mathbf{x} - ct\mathbf{\Omega}_i\|), \tag{39}$$

where the sum over i denotes a sum over all angles. In contrast to the transport and P_N solutions, the S_N solution is a function of both x and y instead of a function of r only. This rotational dependence of the discrete ordinates equations is a factor in the problem called ray effects. In the diffusion case, there is no solution. Eq. 18 is not well defined in a vacuum. The nonlinear (and therefor much harder to solve analytically) flux limited diffusion is defined in a vacuum, and the numeric solution is shown in Figure 2(e).

Figure 2 shows various numerical solutions for the line source problem. All simulations are on a grid two centimeters square with a mesh spacing of about $dx = 0.01\,\mathrm{cm}$. The Monte Carlo simulation in Figure 2(b) is very similar to the transport solution in Figure 2(a), with the exception statistical noise in the solution. This simulation used one hundred thousand particles. It is fairly easy to reduce this noise by simply increasing the number of particles in the simulation[12].

---

[12] But keep in mind Eq. 30 states that to reduce the error by a factor of ten, one hundred times the computer resources must be used.

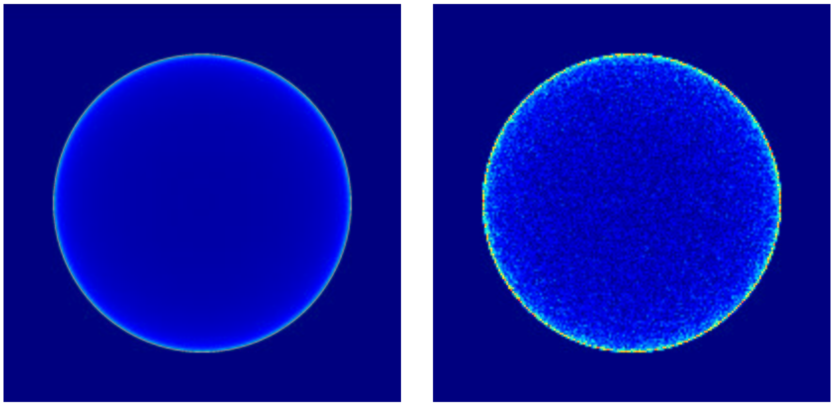

(a) Analytic (b) Monte Carlo

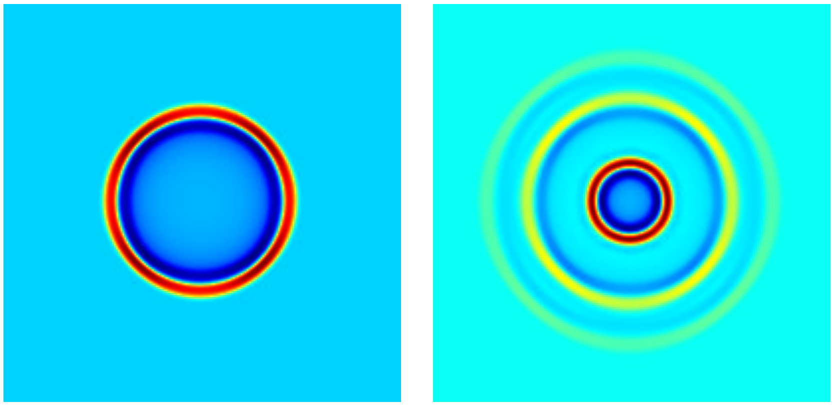

(c) P_1 (d) P_5

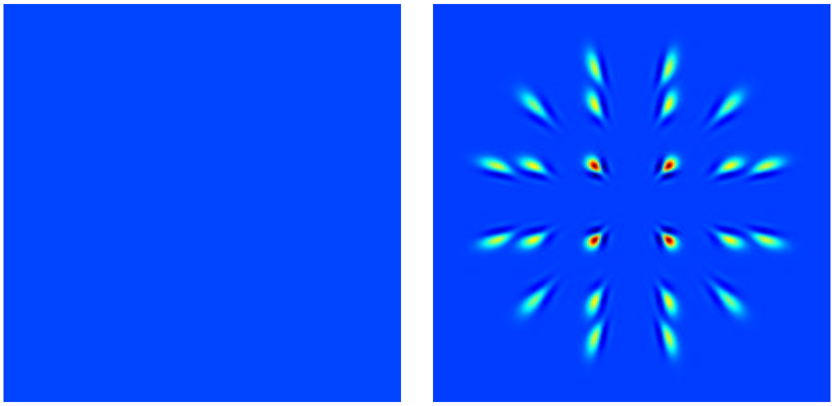

(e) Flux Limited Diffusion (f) S_6

Figure 2: Solutions to the pulsed line source problem. The color scale is linear, and the color at each of the corners equals zero for all approximations except diffusion which uses the same scale as S_6. Colors more blue than the corners are negative.

Figure 2(c) and Figure 2(d) show the P_1 and P_5 solutions, respectively. The P_1 approximation has one wave speed at which particles can travel, whereas P_5 has three wave speeds. This can be seen in the rings moving away from the center. Just behind each ring, there is a negative region in the energy density. Figure 2(e) is not a mistake. The distribution spread out so fast[13] that the distribution is essentially flat and has a very small and nearly uniform value everywhere. A discrete ordinates S_6 calculation is shown in Figure 2(f). Note that the particles are all moving in delta functions away from the center.

The full transport equation is hyperbolic in nature, which means that particles and information can only travel at finite speeds. All of the approximations except diffusion respect this; all of the approximation in Figure 2 have semi-reasonable[14] answers except the diffusion. The key difference between spherical harmonics (P_N) and discrete ordinates (S_N) is that S_N moves particles around along particular beams, giving rise to ray-effects; while P_N moves particles only with particular speeds, giving rise to wave-effects. The Monte Carlo simulation looks the best, but if the problem would have been sensitive to instabilities, the noise in the simulation could be problematic.

Ganapol [19, 20, 21] has analytically solved the transport equation for several other problems in infinite media.

4.2 A Lattice Problem

This problem is a checkerboard of highly scattering and highly absorbing regions loosely based on a small part of a nuclear reactor core. This is only a test of the transport approximations; there is no material energy equation. When an absorption occurs, the particles are simply removed from the system and do not heat it up.

The system for this problem, shown in Figure 3, is seven centimeters wide. The bulk of the lattice is composed of a scattering material with $\sigma_t = \sigma_s = 1\,\mathrm{cm}^{-1}$. There are eleven absorbing regions where $\sigma_t = \sigma_a = 10\,\mathrm{cm}^{-1}$. At time zero, a source of strength one is turned on in the central region of the system. All particles travel at a speed $c = 1\,\mathrm{cm/s}$, and the problem is surrounded on all sides by vacuum boundaries.

Figures 4 and 5 show the energy density E 3.2 seconds after the source is turned on and at steady state (approximately twenty seconds after the source is turned on). In each of the figures, there are results from the diffusion, flux limited diffusion, P_1, P_7, S_6, and implicit Monte Carlo approximations. The diffusion and the discrete ordinates calculations were done with ALEGRA [16]. The implicit Monte Carlo calculation was done using the Kull IMC package [22] and used thirty six million particles in half the problem domain, with a reflective boundary on the center line. The P_N calculations were done with a research code of my own [10, 13].

---

[13] The diffusion length is, after all, infinite.

[14] A "semi-reasonable" answer is one that converges to the correct solution as the order of the method is increased; the results shown in Figures 2(c)-2(f) are by no means truly reasonable.

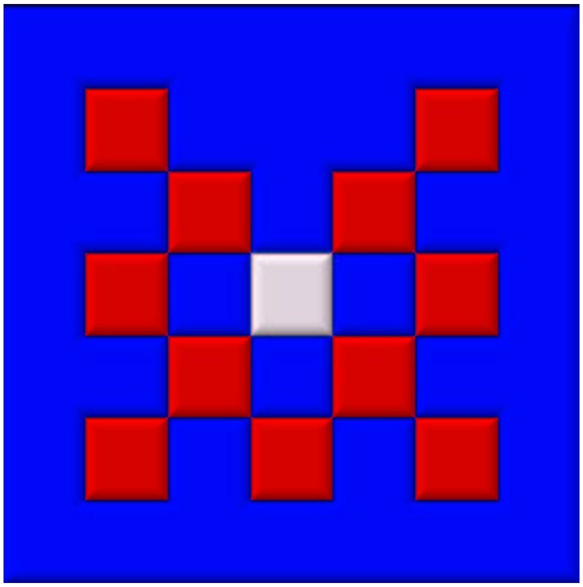

Figure 3: The lattice system. The blue and white regions are pure scattering regions where $\sigma_s = 1\,\mathrm{cm}^{-1}$. Additionally, the white region contains a source of particles. The red regions are pure absorbers with $\sigma_a = 10\,\mathrm{cm}^{-1}$. The particles are simply removed from the system by the absorbers; there is no material equation.

At the early time shown in Figure 4, particles should have had just enough time to reach the boundaries but not enough to reach the corners. The diffusion calculation shown in Figure 4(a) is much too diffuse; the particles have reached all parts of the system. Also, the central region does not have enough particles. The flux limited diffusion result in Figure 4(b) is a vast improvement upon the diffusion calculation and captures the wave front well, but there are no beams of particles leaking between the absorbers as seen in the Monte Carlo and P_7 calculations. The energy density computed using P_1, seen in Figure 4(c), has an artificial wave front of particles traveling at speed $v = 1/\sqrt{3}\,\mathrm{cm/s}$. This is due to the fact that in P_1, the particle waves travel only at this speed. In the P_7 calculation, the particle waves can travel at more speeds, nearly eliminating these nonphysical wave fronts. Some wave-effects can also be seen in the P_7 calculation. Well defined beams of particles leaking between the corners of the absorbing regions in both Figure 4(d) and Figure 4(f), the P_7 and Monte Carlo simulations. Generally P_7 and Monte Carlo agree very well, especially for energy densities above 10^{-4}. The S_6 calculation shown in Figure 4(e) has about the same number of degrees of freedom as the P_7 calculation, but the ray-effects are very dominant.

At steady state, the Monte Carlo and P_7 again agree extremely well. Both Figure 5(d) and Figure 5(f) show distinct shadows in the corners behind the absorbers, as well as prominent beam-like features leaking from between the absorbers. Again these beams cannot be seen in the flux limited diffusion result in Figure 5(b). The P_1 and diffusion results in Figure 5(c) and Figure 5(a) should

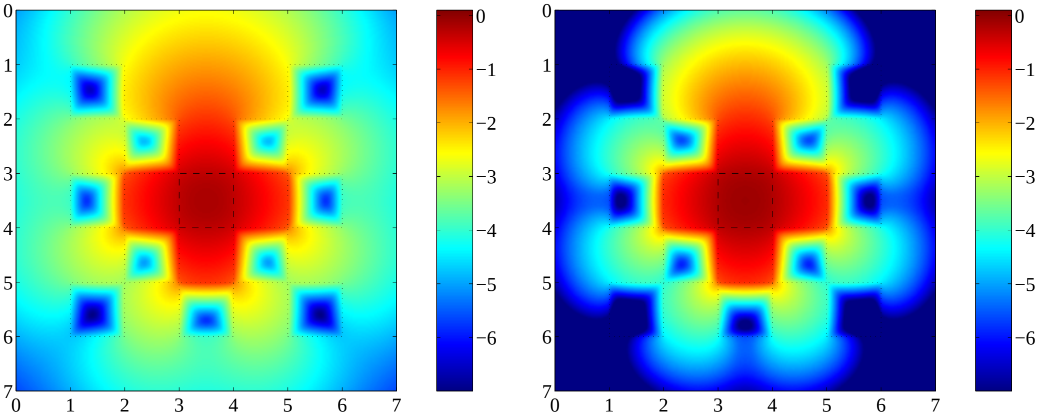

(a) Diffusion (b) Flux limited diffusion

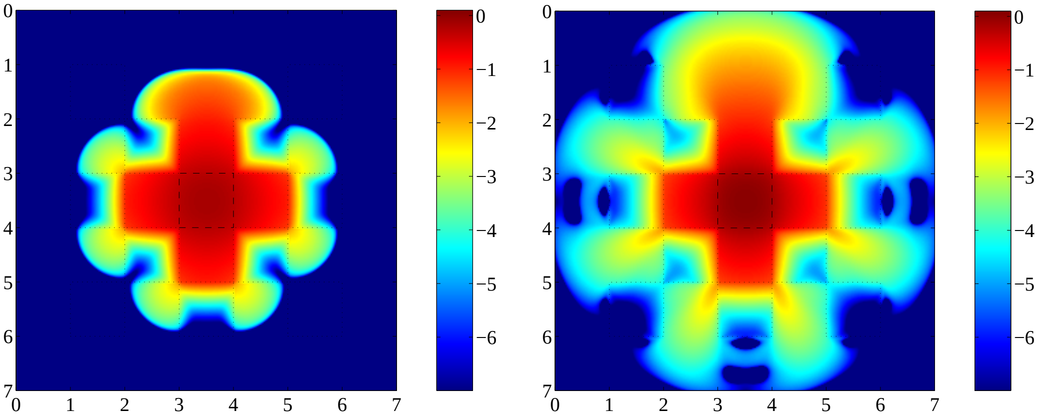

(c) P_1 (d) P_7

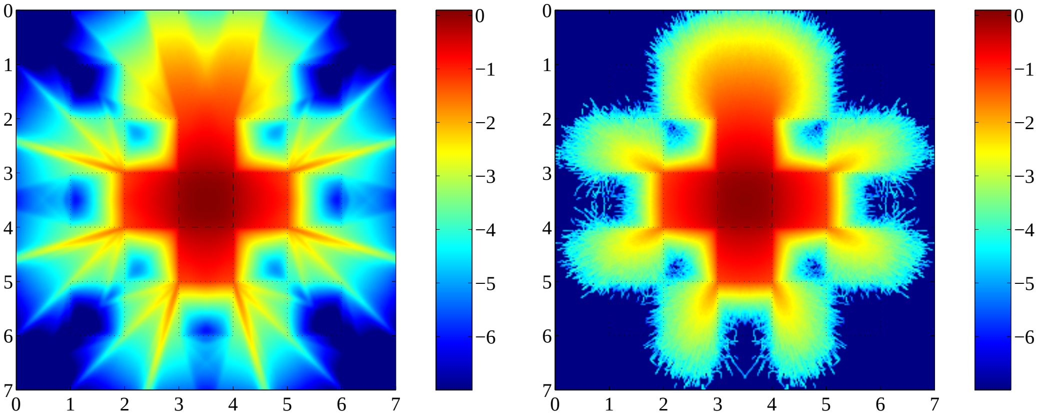

(e) S_6 (f) Implicit Monte Carlo

Figure 4: The calculated energy density in the lattice problem 3.2 seconds after the source was turned on. The color-map is proportional to $\log_{10} E$ and limited to seven orders of magnitude.

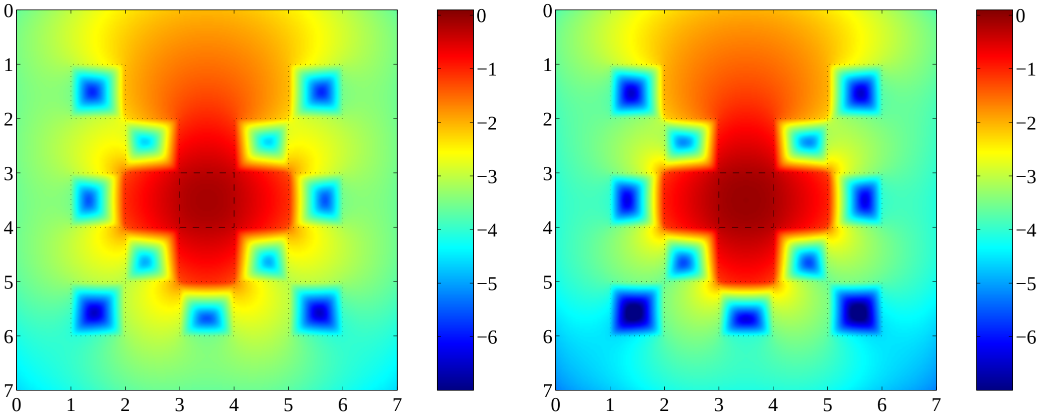

(a) Diffusion

(b) Flux limited diffusion

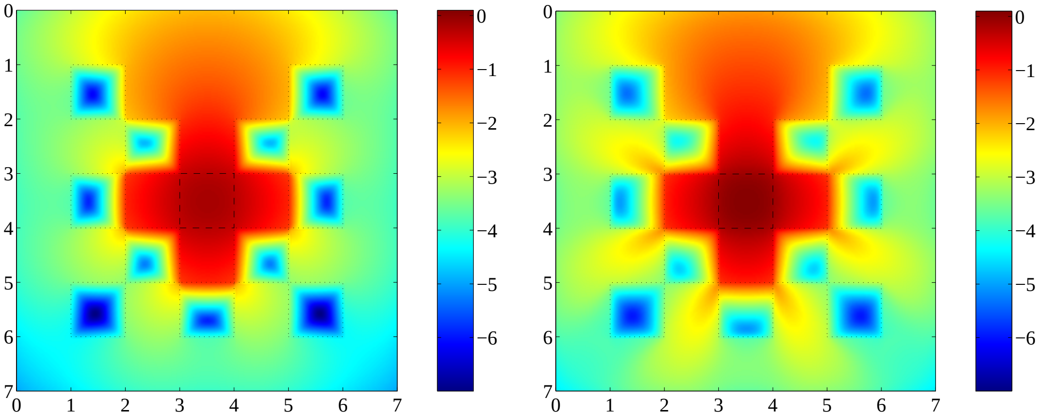

(c) P_1

(d) P_7

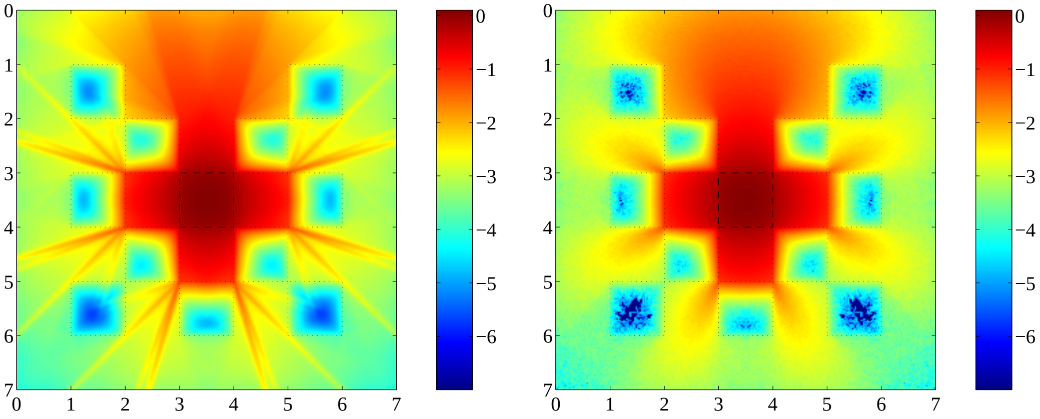

(e) S_6

(f) Implicit Monte Carlo

Figure 5: The calculated energy density in the lattice problem at steady state. The color-map is proportional to $\log_{10} E$.

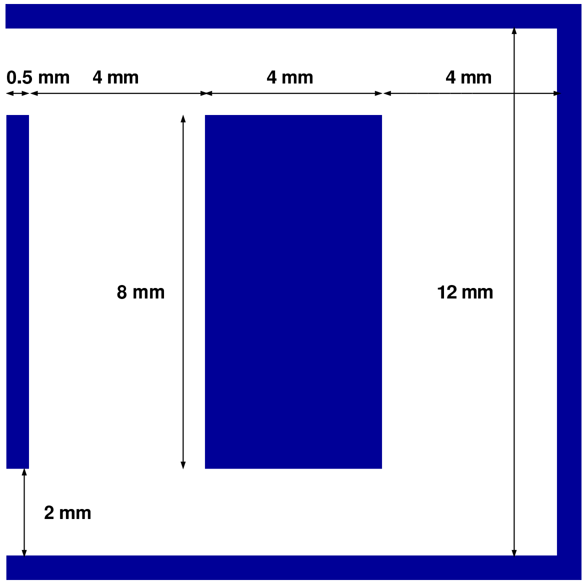

Figure 6: The hohlraum. The blue regions are pure absorbers regions where $\sigma_a = 100\,\mathrm{cm}^{-1}$ and $\rho C_v = 5.0 \times 10^5\ \mathrm{J/m^3\,K}$. the white region is a vacuum.

match, but they do not here because the P_1 code uses a higher order method which essentially gives more resolution on the same grid size as the diffusion calculation. Again, the discrete ordinates solution is dominated by the ray-effects in Figure 5(e), even in steady state. The negative waves in the P_7 solution disappear in steady state in Figure 5(d). This will always be true; the P_N wave-effects always vanish in steady state, while the S_N ray-effects can be present in both time dependent and steady state problems.

4.3 A Hohlraum

This hohlraum problem is loosely based on a typical hohlraum for the Z-machine at Sandia. The radiation field is coupled to the the material energy through Eq. 3. Unlike a real hohlraum, this problem is described in Cartesian coordinates. The system, shown in Figure 6, is thirteen millimeters square with a thin wall of material around the outside edge. There are two two millimeter openings on either left side of the hohlraum, and there is a rectangular block of material in the center of the system. The material is a pure absorber with $\sigma_a = 100\,\mathrm{cm}^{-1}$ and $\rho C_v = 5.0 \times 10^5\ \mathrm{J/m^3\,K}$. The rest of the problem is a vacuum. Some codes used for this problem could not model a pure void, so the heat capacity was set extremely large, $\rho C_v = 1.0 \times 10^{99}\ \mathrm{J/m^3\,K}$. The opacities were all set to zero in the void. The initial material and radiation temperatures were set to $T_0 = 300\,\mathrm{K}$. A source boundary condition is applied along the entire left hand side. The source has a temperature of $T_{\text{source}} = 3.5 \times 10^6\,\mathrm{K}$.

Figures 7-8 show the radiation temperature, as defined by Eq. 8, at times of

$t_1 = 3.93606 \times 10^{-11}\,\mathrm{s}$, and $t_2 = 5.0 \times 10^{-10}\,\mathrm{s}$. The material temperature at $t_2 = 5.0 \times 10^{-10}\,\mathrm{s}$ is shown in Figure 9. Throughout the discussion below, it is assumed that the Implicit Monte Carlo simulation is the most accurate answer.

At the time depicted in Figure 7, photons have had nearly enough time to back wall of the hohlraum. Most of the photons are still streaming from the openings; the walls of the hohlraum have not started to heat up yet. Flux limited diffusion, Figure 7(b) has incorrectly allowed photons to fill the entire system. The P_1 (Figure 7(c)) and P_9 (Figure 7(d)) simulations both have wave-like solutions, which allow the photons to bend around the front wall. Notice the black regions in the P_9 solution in Figure 7(d); these represent negative solutions. While too many photons are transported in the wave front around the back side of the wall, P_9 “tries” to compensate by having waves of negative energy follow the positive waves that should not be there. The P_1 and S_2 solutions are nearly opposites of each other; the P_1 solution in Figure 7(c) is much too uniform while the S_2 solution in Figure 7(e) has particles traveling along distinct beams, which are no traveling in the right direction. The S_8 calculation has many more beams, but it is still suffering badly from ray-effects. While these ray-effects persist even at long times, the wave effects seen in P_9 solution, Figure 7(d), quickly travel through the system.

Finally in Figure 8, the simulation is approaching steady state. Because P_1 was the quickest of the simulation methods used here, it was the basis of a scoping calculation to see how long the simulation should last. Unfortunately its answer is completely wrong; the photon energy density is much to uniform. All of the other approximations are still changing rapidly. Flux limited diffusion is somewhat better, as can be seen in Figure 8(b), but it has still transported too much energy through the problem. In the IMC calculation, Figure 8(a), the back wall is just starting to heat up and re-emit photons. While the P_9 and S_8 simulations are beginning to qualitatively look good, they still are suffering from wave-effects (Figure 8(d)) and ray-effects (Figure 8(f)). In the P_9 simulation, the photon energy density has bled around the corners too much.

The material temperature at the final time of $t = 5.0 \times 10^{-10}\,\mathrm{s}$ is shown in Figure 9. Even thought the photon energy density of the IMC is noisy, the calculated material temperature in Figure 9(a) is much smoother. This is because the individual photons of the simulation have a small effect on the material temperature. It takes many photons to change the temperature by a significant amount. This essentially adds an extra level of averaging in the simulation that dramatically improves the quality of the material temperature over what is expected from the radiation field. Notice that the back side of the capsule has a very uniform temperature; the other higher order methods (S_8 and P_9) are both nonuniform. This could cause problems in instability studies, although the IMC simulation still has some noise, it is just at a much shorter wavelength and smaller amplitude. Again, P_1 and flux limited diffusion have warmed up the walls too much, especially in the right half of the simulation.

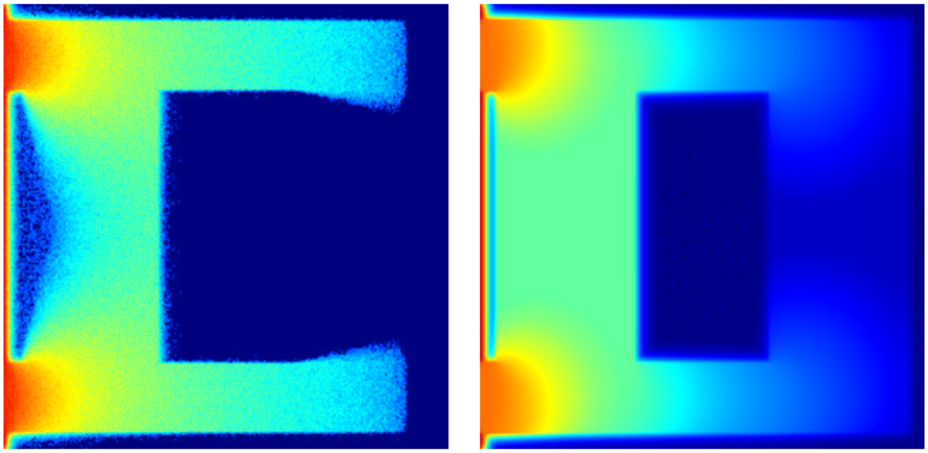

(a) Implicit Monte Carlo (b) Flux limited diffusion

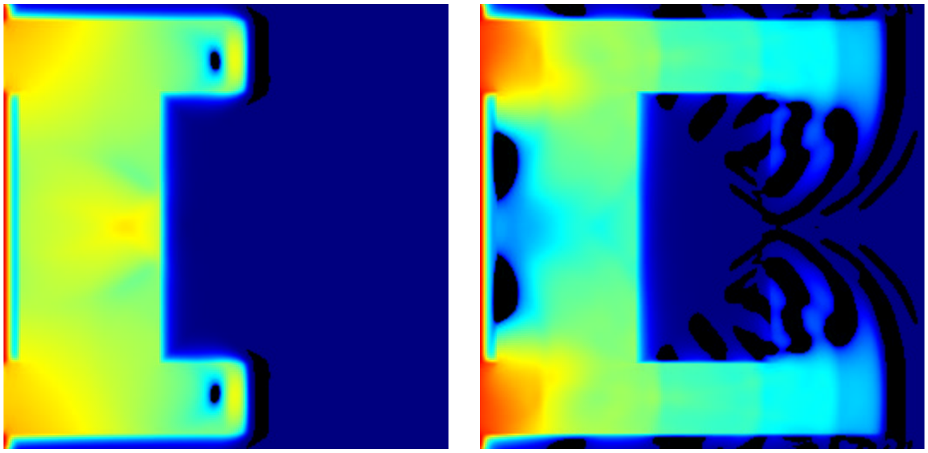

(c) P_1 (d) P_9

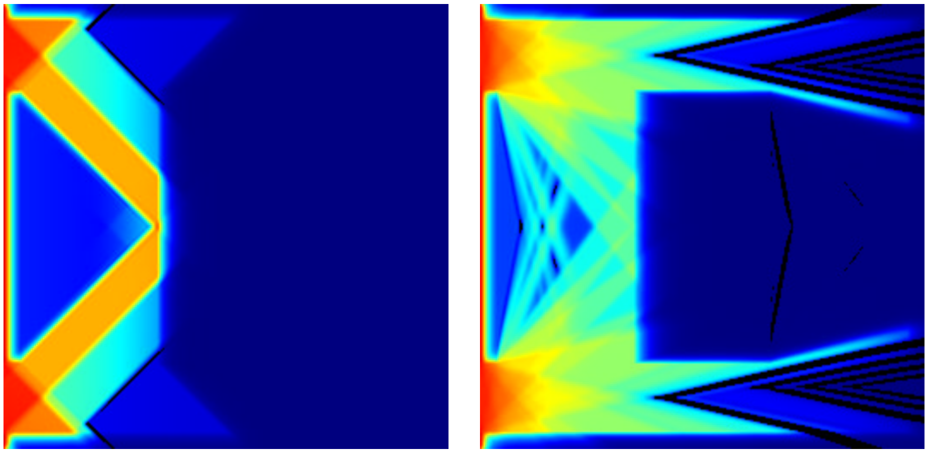

(e) S_2 (f) S_8

Figure 7: The radiation temperature in the hohlraum problem at $t = 3.93606 \times 10^{-11}\,\mathrm{s}$ after the source was turned on. The color-map is proportional to $T_r = (E/a)^{1/4}$. Black regions indicate negative energy densities.

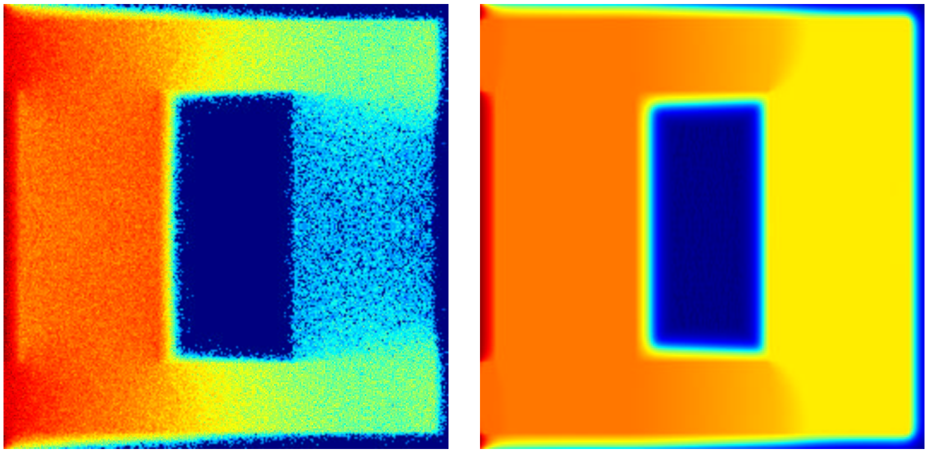

(a) Implicit Monte Carlo (b) Flux limited diffusion

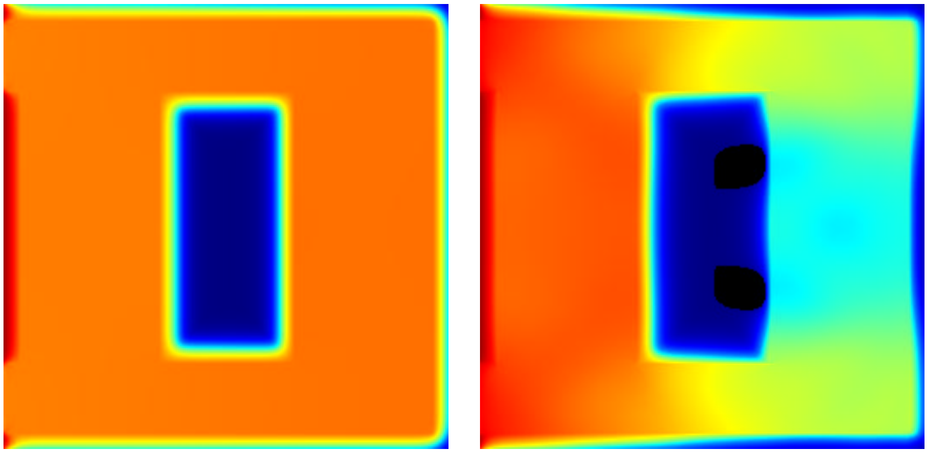

(c) P_1 (d) P_9

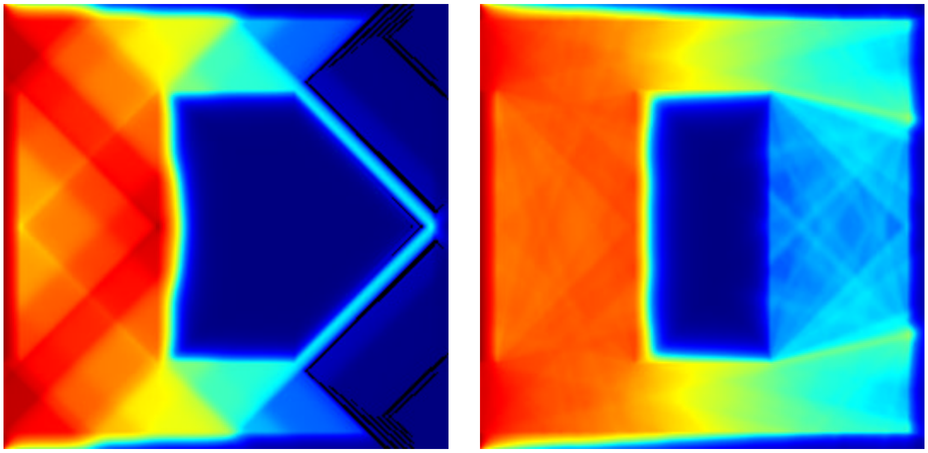

(e) S_2 (f) S_8

Figure 8: The radiation temperature in the hohlraum problem at $t = 5.0 \times 10^{-10}\,\mathrm{s}$ after the source was turned on. The color-map is proportional to $T_r = (E/a)^{1/4}$. Black regions indicate negative energy densities.

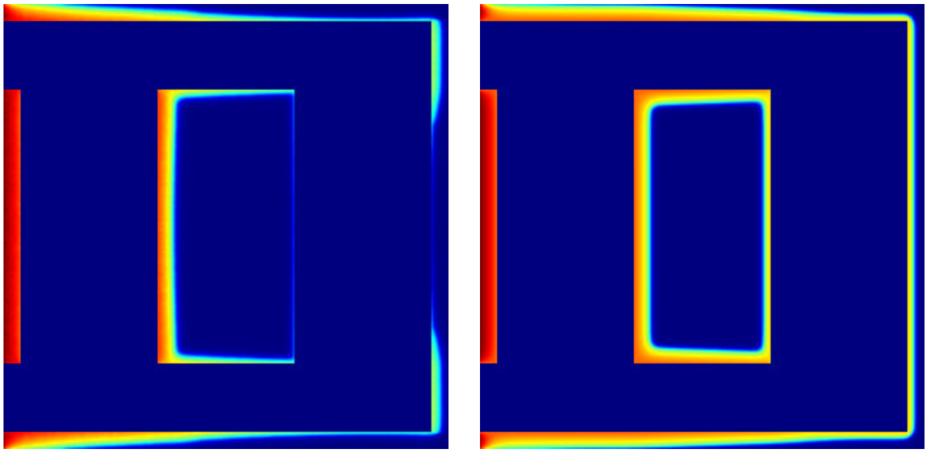

(a) Implicit Monte Carlo (b) Flux limited diffusion

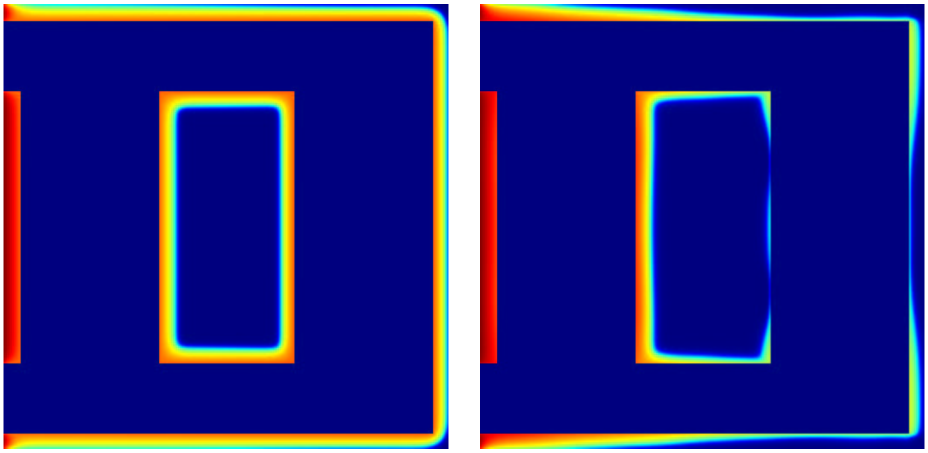

(c) P_1 (d) P_9

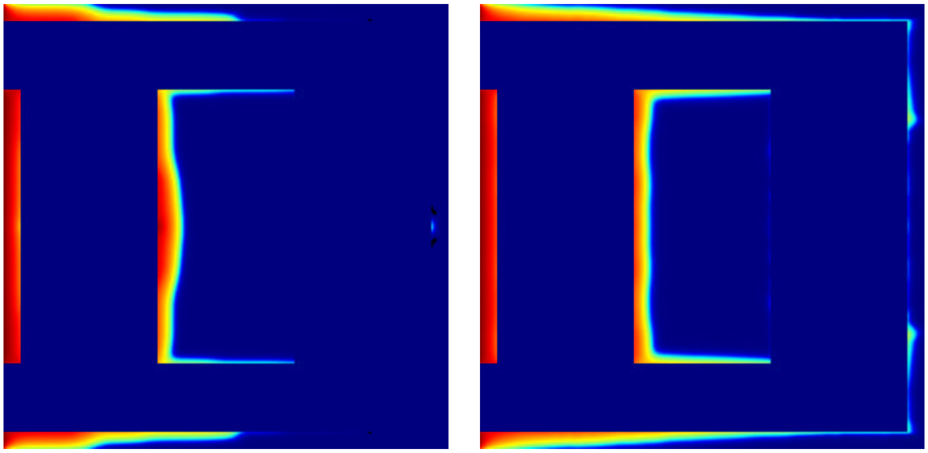

(e) S_2 (f) S_8

Figure 9: The material temperature in the hohlraum problem at $t = 5.0 \times 10^{-10}\,\mathrm{s}$ after the source was turned on. The color-map is proportional to T_m.

5 Conclusions

Simulating radiation transport is difficult; the equation we would really like to use, the Boltzmann transport equation, is seven dimensional. This leads to a myriad of different approximations to the transport equation.[15]

Diffusion is by far the simplest approximation and works well when there is material for the photons to diffuse through. The many varieties of flux limited diffusion all attempt to improve upon plane diffusion while remaining fairly easy to solve. The errors with diffusion theory all stem from the fact that the fundamental mathematical characteristic of the transport has been changed from hyperbolic to parabolic. This change means that photons are no longer constrained to travel at the speed of light. Some extremely fast and robust numerical methods have been developed to numerically solve the diffusion theory equations.

The spherical harmonics approximation takes moments of the Boltzmann equation to arrive at a set of conservation laws for each of the moments. In a vacuum, this approximation leads to the wave equations, and this causes the simulations to suffer from wave-effects. Theoretically these effects become negligible when enough moments are used, but in a vacuum, an infinite number of moments are needed to eliminate the wave-effects.

The discrete ordinates approximation moves photons only along a particular set of directions. Many people have studied this approximation, making its problems well understood. Many very efficient algorithms have been developed to solve the discrete ordinates equations. Unfortunately, ray-effects, the most well-known defect of discrete ordinates, can be seen in many simulations.

Implicit Monte Carlo can treat photons exactly, but a given simulation cannot come close to simulating as many particles as there are in all physical systems. This leads to statistical noise, which is this method's largest weakness. In order to reduce the amount of noise in a given simulation by a factor of ten, one hundred times more particles must be simulated. In time-dependent problems, not only does this increase run-time by a factor of one hundred, but memory usage also increases by the same factor. The resulting material energy calculated in an IMC simulation, however, is much less noisy than the radiation field, and it is usually the material energy that is more important for simulations.

For the test problems in this paper, the Monte Carlo generally gave the best results. Flux limited diffusion gave the best results normalized by run time. Spherical harmonics and discrete ordinates both have some significant problems in optically thin materials, but spherical harmonics appears to perform slightly better in highly heterogeneous material such as the lattice problem.

---

[15] This is lucky for PhD students, who's advisor's love coming up with new approximations.

References

[1] J. W. Bates, D. A. Knoll, W. J. Rider, R. B. Lowrie, and V. A. Mousseau. "On Consistent Time-Integration Methods for Radiation Hydrodynmaics in the Equilibrium Diffusion Limit: Low-Energy-Density Regime." *Journal of Computational Physics*, vol. 167(1), pp. 99–130, February 2001.

[2] G. I. Bell and S. Glasstone. *Nuclear Reactor Theory*. Krieger, 1970. ISBN 0-88275-790-3.

[3] D. Blatner. *The Joy of π*. Walker, 1997. ISBN 0802713327. URL `http://www.joyofpi.com`.

[4] P. N. Brown and B. Chang. "On the Use of Diffusion Synthetic Acceleration in Parallel 3D Neutral Particle Transport Calculations." Tech. Rep. UCRL-JC-130877, Lawrence Livermore National Laboratory, Livermore, CA, 1998.

[5] P. N. Brown, B. Chang, F. Graziani, and C. S. Woodward. "Implicit Solution of Large-Scale Radiation-Material Energy Transfer Problems." *Iterative Methods in Scientific Computation II*, pp. 1–14, 1999.

[6] P. N. Brown, F. Graziani, I. Otero, and C. S. Woodward. "Implicit Solution of Large-Scale Radiation Diffusion Problems." Tech. Rep. UCRL-JC-141881, Lawrence Livermore National Laboratory, Livermore, CA, 2001.

[7] P. N. Brown and U. R. Hanebutte. "Spherical Harmonics Solutions to the 3D Kobayashi Benchmark Suite." In "PHYSOR 2000, ANS International Topical Meeting on the Advances in Reactor Physics and Mathematics and Computation into the Next Millennium," American Nuclear Society, May 2000.

[8] P. N. Brown, A. C. Hindmarsh, and L. R. Petzold. "Using Krylov Methods in the Solution of Large-Scale Differential-Algebraic Systems." *SIAM Journal on Scientific Computing*, vol. 15(6), pp. 1467–1488, November 1994.

[9] P. N. Brown and C. S. Woodward. "Preconditioning Strategies for Fully Implicit Radiation Diffusion with Material-Energy Transfer." *SIAM Journal on Scientific Computing*, vol. 23(2), pp. 499–516, August 2001.

[10] T. A. Brunner. *Riemann Solvers for Time-Dependent Transport Based on the Maximum Entropy and Spherical Harmonics Closures*. Ph.D. thesis, University of Michigan, 2000.

[11] T. A. Brunner and J. P. Holloway. "Two New Boundary Conditions for Use with the Maximum Entropy Closure and an Approximate Riemann Solver." In "PHYSOR 2000, ANS International Topical Meeting on the Advances in Reactor Physics and Mathematics and Computation into the Next Millennium," American Nuclear Society, May 2000.

[12] T. A. Brunner and J. P. Holloway. "One-Dimensional Riemann Solvers and the Maximum Entropy Closure." *Journal of Quantitative Spectroscopy and Radiative Transfer*, vol. 69, pp. 543–566, 2001.

[13] T. A. Brunner and J. P. Holloway. "Two Dimensional Time Dependent Riemann Solvers for Neutron Transport." In "M&C 2001 Salt Lake City," American Nuclear Society, September 2001.

[14] T. A. Brunner, J. P. Holloway, and E. W. Larsen. "On the Use of Maximum Entropy Eddington Factors in Shielding Calculations." *Transactions of the American Nuclear Society*, vol. 77, pp. 195–196, Nov 1997.

[15] T. A. Brunner, J. P. Holloway, and K. G. Powell. "Using an Approximate Riemann Solver with the Maximum Entropy Closure." *Transactions of the American Nuclear Society*, vol. 79, pp. 128–129, Nov 1998.

[16] K. G. Budge. "Verification of the Radiation Package in ALEGRA." Tech. Rep. SAND99-0786, Sandia National Laboratory, Albuquerque, NM, 1999.

[17] J. A. Fleck, Jr. and J. D. Cummings. "An Implicit Monte Carlo Scheme for Calculating Time and Frequency Dependent Nonlinear Radiation Transport." *Journal of Computational Physics*, vol. 8, pp. 313–342, 1971.

[18] D. R. Fokkema, G. L. G. Sleijpen, and H. A. V. D. Vorst. "Accelerated Inexact Newton Schemes For Large Systems of Nonlinear Equations." *SIAM Journal on Scientific Computing*, vol. 19(2), pp. 657–674, Mar 1998.

[19] B. D. Ganapol. "Solution of the One-Group Time-Dependent Neutron Transport Equation in and Infinite Medium by Polynomial Reconstruction." *Nuclear Science and Engineering*, vol. 92, pp. 272–279, 1986.

[20] B. D. Ganapol. *Homogeneous Infinite Media Time-Dependent Analytic Benchmarks for X-TM Transport Methods Development*. Los Alamos National Laboratory, Mar 1999.

[21] B. D. Ganapol and K. L. Peddicord. "The Generation of Time-Dependent Neutron Transport Solutions in Infinite Media." *Nuclear Science and Engineering*, vol. 64, pp. 317–331, 1977.

[22] N. A. Gentile, N. Keen, and J. Rathkopf. "The KULL IMC Package." Tech. Rep. UCRL-JC-132743, Lawrence Livermore National Laboratory, Livermore, CA, 1998.

[23] J. D. Huba. "NRL Plasma Formulary." Tech. Rep. NRL/PU/6790–00-426, Naval Research Laboratory, Washington, DC 20375-5320, 2000. URL `http://wwwppd.nrl.navy.mil/nrlformulary/index.html`.

[24] J. Jung, H. Chijiwa, K. Kobayashi, and H. Nishihara. “Discrete Ordinate Neutron Transport Equation Equivalent to P_L Approximation.” *Nuclear Science and Engineering*, vol. 49, p. 1, 1972.

[25] D. S. Kershaw. “Flux Limiting Nature’s Own Way.” Tech. Rep. UCRL-78378, Lawrence Livermore National Laboratory, Livermore, CA, 1976.

[26] D. A. Knoll and W. J. Rider. “A Multigrid Preconditioned Newton-Krylov Method.” *SIAM Journal on Scientific Computing*, vol. 21(2), pp. 691–710, October 1999.

[27] D. A. Knoll, W. J. Rider, and G. L. Olson. “An Efficient Nonlinear Solution Method for Non-equilibrium Radiation Diffusion.” *Journal of Quantitative Spectroscopy and Radiative Transfer*, vol. 63(1), pp. 15–29, September 1999.

[28] D. A. Knoll, W. J. Rider, and G. L. Olson. “Nonlinear Convergence, Accuracy, and Time Step Control in Nonequilibrium Radiation Diffusion.” *Journal of Quantitative Spectroscopy and Radiative Transfer*, vol. 152(1), pp. 25–36, July 2001.

[29] R. J. LeVeque, D. Mihalas, E. A. Dorfi, and E. Müller. *Computational Methods for Astrophysical Fluid Flow*. Springer, 1998. ISBN 3-540-64448-2.

[30] C. D. Levermore. “Relating Eddington Factors to Flux Limiters.” *Journal of Quantitative Spectroscopy and Radiative Transfer*, vol. 31, pp. 149–160, 1984.

[31] C. D. Levermore and G. C. Pomraning. “A Flux-Limited Diffusion Theory.” *The Astrophysical Journal*, vol. 248, pp. 321–334, August 1981.

[32] E. E. Lewis and W. F. Miller, Jr. *Computational Methods of Neutron Transport*. American Nuclear Society, 1993. ISBN 0-89448-452-4.

[33] D. Mihalas and B. Weibel-Mihalas. *Foundations of Radiation Hydrodynamics*. Dover, 1999. ISBN 0-486-40925-2.

[34] W. F. Miller and W. H. Reed. “Ray-Effect Mitigation Methods for Two-Dimensional Neutron Transport Theory.” *Nuclear Science and Engineering*, vol. 62, p. 391, 1977.

[35] G. N. Minerbo. “Maximum Entropy Eddington Factors.” *Journal of Quantitative Spectroscopy and Radiative Transfer*, vol. 20, p. 541, 1978.

[36] P. J. Mohr and B. N. Taylor. “CODATA Recommended Values of the Fundamental Physical Constants: 1998.” Tech. rep., National Institute of Standards and Technology, Gaithersburg, MD 20899-8401. URL `http://www.physics.nist.gov/cuu/Constants/index.html`.

[37] V. A. Mousseau, D. A. Knoll, and W. J. Rider. "Physics-Based Preconditioning and the Newton-Krylov Method for Non-equilibrium Radiation Diffusion." *Journal of Computational Physics*, vol. 160(2), pp. 743–765, May 2000.

[38] G. L. Olson, L. H. Auer, and M. L. Hall. "Diffusion, P1, and Other Approximate Forms of Radiation Transport." *Journal of Quantitative Spectroscopy and Radiative Transfer*, vol. 64(6), pp. 619–634, March 2000.

[39] G. C. Pomraning. *The Equations of Radiation Hydrodynamics*. Pergamon Press, 1973. ISBN 0-08-016893-0.

[40] W. H. Reed. "Spherical Harmonic Solutions of the Neutron Transport Equation from Discrete Ordinate Codes." *Nuclear Science and Engineering*, vol. 49, p. 10, 1972.

[41] W. J. Rider and D. A. Knoll. "Time Step Size Selection for Radiation Diffusion Calculations." *Journal of Computational Physics*, vol. 152(2), pp. 790–795, July 1999.

[42] W. J. Rider, D. A. Knoll, and G. L. Olson. "Multigrid Newton-Krylov Method for Multimaterial Equilibrium Radiation Diffusion." *Journal of Computational Physics*, vol. 152(1), pp. 164–191, June 1999.

[43] A. I. Shestakov, J. L. Milovich, and M. K. Prasad. "Combining Cell- and Point-Centered Methods in 3D, Unstructured-Grid Radiation-Hydrodynamic Codes." *Journal of Computational Physics*, vol. 170, pp. 81–111, 2001.

[44] B. Su. "Variable Eddington Factors and Flux Limiters in Radiative Transfer." *Nuclear Science and Engineering*, vol. 137, pp. 281–297, March 2001.

[45] P. Wang. "Computation and Application of Atomic Data for Interial Confinement Fusion Plasmas." Tech. Rep. UWFDM-855, Fusion Technology Institute, University of Wisconsin, Madison, Wisconsin, June 1991. Also Ph.D. Thesis.

[46] J. S. Warsa, T. A. Wareing, and J. E. Morel. "Fully Consistent Diffusion Synthetic Acceleration of Linear Discontinuous Transport Discretizations on Three-Dimensional Unstructured Meshes." Tech. rep., Los Alamos National Laboratory, Los Alamos, New Mexico. URL `http://lib-www.lanl.gov/la-pubs/00818582.pdf`.

[47] Wesley C. Fan and Clifton R. Drumm and Jeniffer L Powell. "Discrete Ordinates Approximations to the First- and Second-Order Radiation Transport Equations." Tech. Rep. SAND2002-1880, Sandia National Laboratories, Jun 2002.

A Boundary Conditions

The most physically relevant boundary conditions for a radiation transport problem specify the radiation entering the system, known as a source boundary condition. We generally do not know how much radiation is exiting a system before the calculation begins, so it remains unspecified. We can specify the incoming radiation mathematically for use in the Boltzmann, Eq. 2, as

$$I(\mathbf{\Omega}_{\text{in}}) = i(\mathbf{\Omega}_{\text{in}}), \tag{40}$$

where $\mathbf{\Omega}_{\text{in}} \cdot \mathbf{n} < 0$, $\mathbf{n}$ is the outward surface normal, and $i(\mathbf{\Omega}_{\text{in}})$ is the specified incoming radiation. If the incoming radiation is zero,

$$I(\mathbf{\Omega}_{\text{in}}) = 0, \tag{41}$$

then this boundary condition is known as a vacuum boundary.

Another useful, but purely mathematical, boundary condition is a reflecting boundary condition. The reflecting boundary condition allows the simulation to exploit planes of symmetry so that only a small part of the physical system needs to be simulated. This can save a considerable amount of computer time. At the reflecting boundary we have

$$I(\mathbf{\Omega}) = I(\mathbf{\Omega} - (2\mathbf{\Omega} \cdot \mathbf{n})\mathbf{n}), \tag{42}$$

where again $\mathbf{n}$ is the outward surface normal. An extension of the reflective boundary is the albedo boundary condition where only a fraction of the outgoing radiation is reflected back into the system. This can be expressed as

$$I(\mathbf{\Omega}_{\text{in}}) = \alpha I(\mathbf{\Omega}_{\text{in}} - (2\mathbf{\Omega}_{\text{in}} \cdot \mathbf{n})\mathbf{n}), \tag{43}$$

where again $\mathbf{\Omega}_{\text{in}} \cdot \mathbf{n} < 0$, and $0 \leq \alpha \leq 1$ is the albedo. When $\alpha = 0$ the albedo boundary condition is the same as the vacuum boundary condition, and if $\alpha = 1$, the reflective boundary condition is recovered.

A final class of boundary conditions is the Dirichlet boundary condition. Here, the radiation field is completely specified along a particular boundary.

$$I(\mathbf{\Omega}) = i(\mathbf{\Omega}), \tag{44}$$

where $i(\mathbf{\Omega})$ is a given function. Dirichlet boundary conditions are most useful for comparing analytic answers with numerical solutions.

Each of the approximations to the Boltzmann equation, Eq. 2, must also approximate the natural boundary conditions described in Eqs. 40-44. In discrete ordinates, each of the boundary conditions is averaged over an angular range and assigned to the corresponding beam. Diffusion and spherical harmonics are a bit harder. Various moments of the specified boundary condition must be taken to specify the moments in the simulation. This will be explicitly done for diffusion in the next section.

Diffusion Boundary Conditions

Only regular diffusion will be considered here. The details for flux limited diffusion can be found in a paper by Levermore and Pomraning [31].

Since the diffusion approximation is posed in terms of integral quantities of the intensity I, the boundary conditions must also be approximated by integral quantities. The mostly widely used boundary condition is a Marshak boundary condition in which the incoming partial flux is specified. The incoming flux is defined as

$$F_{\text{in}} = -\int_{\mathbf{\Omega}\cdot\mathbf{n}<0} \mathbf{n}\cdot\mathbf{\Omega} I \,\mathrm{d}\mathbf{\Omega}\,. \tag{45}$$

Inserting the diffusion approximation of I from Eq. 13 into Eq. 45 yields

$$F_{\text{in}} = \frac{1}{4}E - \frac{1}{2}\mathbf{n}\cdot\mathbf{F}. \tag{46}$$

We can also define an outgoing flux by integrating Eq. 45 over $\mathbf{\Omega}\cdot\mathbf{n} > 0$,

$$F_{\text{out}} = \frac{1}{4}E + \frac{1}{2}\mathbf{n}\cdot\mathbf{F}. \tag{47}$$

With these two partial fluxes and recalling that $\mathbf{F} = -1/3\sigma_t\nabla E$, we can reconstruct all the transport boundary conditions.

The source boundary condition (Eq. 40) is simply

$$F_{\text{in}} = \frac{1}{4}E - \frac{1}{2}\mathbf{n}\cdot\mathbf{F} = f \tag{48}$$

where f is the specified incoming flux. Setting $f = 0$ is the vacuum boundary. Usually the incoming flux is given in terms of a temperature. In this case, setting $i = B(T_{\text{source}})$ in Eq. 45 yields

$$F_{\text{in}} = \frac{1}{4}E - \frac{1}{2}\mathbf{n}\cdot\mathbf{F} = \frac{1}{4}B_E(T_{\text{source}}). \tag{49}$$

For an albedo boundary condition we know that $F_{\text{in}} = \alpha F_{\text{out}}$, where α is the fraction of radiation that is reflected back into the system. With this, we get the condition

$$-\frac{1}{2}\frac{1-\alpha}{1+\alpha}E + \mathbf{n}\cdot\mathbf{F} = 0. \tag{50}$$

We can easily recover the reflective boundary condition by setting $\alpha = 1$ to get

$$\mathbf{n}\cdot\mathbf{F} = 0. \tag{51}$$

A Dirichlet boundary condition is trivial, we simply set $E = E_0$ along the boundary.

Inspection of the diffusion boundary conditions reveals that they can all be written in the same form as

$$\mathcal{A}E + \mathcal{B}\mathbf{n}\cdot\mathbf{F} = \mathcal{C}. \tag{52}$$

Table 3 lists the factors $\mathcal{A}$, $\mathcal{B}$, and $\mathcal{C}$ for all the boundary conditions listed here.

Boundary Condition	$\mathcal{A}$	$\mathcal{B}$	$\mathcal{C}$
Dirichlet	1	0	E_0
Vacuum	$-1/2$	1	0
Source	$-1/2$	1	$-2F_{\text{in}} = -B_E(T_{\text{source}})/2$
Reflection	0	1	0
Albedo	$-(1-\alpha)/2(1+\alpha)$	1	0

Table 3: Coefficients for the diffusion boundary conditions.

Constant	**SI**	**CGS**
Speed of light, c	$2.99792458 \times 10^{8}\,\text{m/s}$	$2.99792458 \times 10^{10}\,\text{cm/s}$
Planck, h	$6.62606876 \times 10^{-34}\,\text{J s}$	$6.62606876 \times 10^{-27}\,\text{erg s}$
Boltzmann, k	$1.3806503 \times 10^{-23}\,\text{J/K}$	$1.3806503 \times 10^{-16}\,\text{erg/K}$
	$1.6021764 \times 10^{-19}\,\text{J/eV}$	$1.6021764 \times 10^{-12}\,\text{erg/eV}$
	$(1.1604506 \times 10^{4}\,\text{K/eV})$	$(8.617342 \times 10^{-5}\,\text{eV/K})$
Black Body, a	$7.565766 \times 10^{-16}\,\text{J/m}^3\,\text{K}^4$	$7.565766 \times 10^{-15}\,\text{erg/cm}^3\,\text{K}^4$
	$1.372017 \times 10^{1}\,\text{J/m}^3\,\text{eV}^4$	$1.372017 \times 10^{2}\,\text{erg/cm}^3\,\text{eV}^4$
Stefan-Boltzmann, σ	$5.670400 \times 10^{-8}\,\text{W/m}^2\,\text{K}^4$	$5.670400 \times 10^{-5}\,\text{erg/cm}^2\,\text{K}^4\,\text{s}$
	$1.028301 \times 10^{9}\,\text{W/m}^2\,\text{eV}^4$	$1.028301 \times 10^{12}\,\text{erg/cm}^2\,\text{eV}^4\,\text{s}$

Table 4: Physical constants used in radiation transport.

B Physical Constants

Various unit systems are commonly used in radiation transport. Both SI and CGS are used, as well as modifications on each of these where the energy and temperature units are replaced by electron Volts (eV). Table 4 lists the constants for different unit systems. All constants are listed with as many significant digits as are known. This means that any calculation can only be good to roughly the first six decimal places. The National Institute of Standards and Technology has a very good website tabulating all physical constants [36]. Another source for units of most physical quantities, is the NRL Plasma Formulary [23].

The black body constant is defined as

$$a = \frac{8\pi^5 k^4}{15 h^3 c^3}, \tag{53}$$

and the Stefan-Boltzmann constant is defined as

$$\sigma = \frac{ca}{4} = \frac{2\pi^5 k^4}{15 h^3 c^2}. \tag{54}$$

It is standard practice to quote very high temperatures in terms of electron Volts instead of Kelvin. The conversion to Kelvin from electron Volts is accomplished by applying

$$T_{\text{eV}} = kT_{\text{K}}, \tag{55}$$

where T_{eV} is the temperature in electron Volts and T_{K} is the temperature in Kelvin.

The first forty digits [3] of π are

$$\pi = 3.141592653589793238462643383279502884197\ldots \tag{56}$$

C Coordinate Systems

Throughout this paper, the details of the derivative operators in various coordinate systems have been avoided, mostly because they are unimportant for understanding the different approximations. Here, the streaming term from Eq. 1 and the diffusion term from Eq. 18 are explicitly written for various coordinate systems for reference [2].

The Streaming Term

In Cartesian coordinates, the streaming term from Eq. 1 is

$$\mathbf{\Omega} \cdot \nabla f = \sin\vartheta \cos\varphi \frac{\partial}{\partial x} f + \sin\vartheta \sin\varphi \frac{\partial}{\partial y} f + \cos\vartheta \frac{\partial}{\partial z} f \tag{57}$$

The position is given by $\mathbf{r} = (x, y, z)$ and the angle in terms of ϑ and φ. The direction cosines are given by $\mathbf{\Omega} = (\sin\vartheta\cos\varphi, \sin\vartheta\sin\varphi, \cos\vartheta)$. This is the same for all three coordinate systems mentioned here.

In cylindrical coordinates the conservative form of the streaming term is

$$\mathbf{\Omega} \cdot \nabla f = \frac{\sin\vartheta\cos\varphi}{r} \frac{\partial}{\partial r} r f + \frac{\sin\vartheta\sin\varphi}{r} \frac{\partial}{\partial \theta} f + \cos\vartheta \frac{\partial}{\partial z} f - \frac{\sin\vartheta}{r} \frac{\partial}{\partial \varphi} \sin\varphi f, \tag{58}$$

where $\mathbf{r} = (r, \theta, z)$ are the spatial coordinates and (ϑ, φ) are the angular coordinates. ϑ is the angle measured from the z-axis and φ is the angle between the **r**-**z** plane and the **r**-$\mathbf{\Omega}$ plane. This means the direction of $\varphi = 0$ changes with θ and leads to the term with the derivative in φ.

In spherical coordinates where $\mathbf{r} = (r, \theta, \phi)$ and the angles are given by (ϑ,φ), the streaming term is

$$\begin{aligned} \mathbf{\Omega} \cdot \nabla f = \frac{\cos\vartheta}{r^2} \frac{\partial}{\partial r} r^2 f + \frac{\sin\vartheta\sin\varphi}{r\sin\theta} \frac{\partial}{\partial \phi} f + \frac{\sin\vartheta\cos\varphi}{r\sin\theta} \frac{\partial}{\partial \theta} \sin\theta f \\ - \frac{1}{r\sin\vartheta} \frac{\partial}{\partial \vartheta} \sin^2\vartheta f - \frac{\sin\vartheta\cot\theta}{r} \frac{\partial}{\partial \varphi} \sin\varphi f \end{aligned} \tag{59}$$

Here $\cos\vartheta = \mathbf{\Omega} \cdot \hat{\mathbf{r}}$ and φ is the angle between the $\mathbf{\Omega}$-**r** and $\hat{\mathbf{r}}$-$\hat{\mathbf{z}}$ planes.

The Diffusion Operator

The diffusion operator in Eq. 18 in Cartesian coordinates is

$$\nabla \cdot D\nabla E = \frac{\partial}{\partial x} D \frac{\partial}{\partial x} E + \frac{\partial}{\partial y} D \frac{\partial}{\partial y} E + \frac{\partial}{\partial z} D \frac{\partial}{\partial z} E. \tag{60}$$

In cylindrical coordinates when integrating over all angles, the derivatives in angle in Eq. 58 vanish and we have

$$\nabla \cdot D\nabla E = \frac{1}{r} \frac{\partial}{\partial r} r D \frac{\partial}{\partial r} E + \frac{1}{r^2} \frac{\partial}{\partial \theta} D \frac{\partial}{\partial \theta} E + \frac{\partial}{\partial z} D \frac{\partial}{\partial z} E. \tag{61}$$

In spherical coordinates the diffusion term is

$$\nabla \cdot D\nabla E = \frac{1}{r^2} \frac{\partial}{\partial r} r^2 D \frac{\partial}{\partial r} E + \frac{1}{r^2 \sin\theta} \frac{\partial}{\partial \theta} \sin\theta D \frac{\partial}{\partial \theta} E + \frac{1}{r^2 \sin^2\theta} \frac{\partial}{\partial \phi} \sin\theta D \frac{\partial}{\partial \phi} E. \tag{62}$$

Distribution:

1		Nick Gentile L-038 PO Box 808 Livermore, CA 94551
3		James Paul Holloway Department of Nuclear Engineering and Radiological Sciences University of Michigan Cooley Building, North Campus 2355 Bonisteel Blvd. Ann Arbor, MI, 48109-2104
5	MS 1186	T. A. Brunner, 1674
1	1186	R. B. Campbell, 1674
1	1186	K. R. Cochrane, 1674
1	1186	M. P. Desjarlais, 1674
1	1186	T. A. Haill, 1674
1	1186	R. J. Lawrence, 1674
1	1186	R. W. Lemke, 1674
1	1186	T. A. Mehlhorn, 1674
1	1186	B. V. Oliver, 1674
1	1186	S. A. Slutz, 1674
1	1186	W. S. Varnum, 1674
1	1186	R. A. Vesey, 1674
1	1186	E. C. Wemlinger, 1674
1	1186	E. P. Yu, 1674
1	1191	M. K. Matzen, 1600
1	0819	E. A. Boucheron, 9231
1	0819	K. G. Budge, 9231
1	0819	D. E. Carroll, 9231
1	0819	M. A. Christon, 9231
1	0819	C. J. Garasi, 9231
1	0819	A. C. Robinson, 9231
1	0819	M. I. Chen, 9231
1	0819	T. G. Trucano, 9211
1	0316	C. C. Ober, 9233
1	0316	R. P. Pawlowski, 9233
1	1110	J. N. Shadid, 9233
1	1110	T. L. Barth, 9214
1	9217	J. J. Hu, 9214
1	1179	B. C. Franke, 15341
1	1179	L. Lorence, 15341
1	1196	G. A. Rochau, 1677
1	9018	Central Technical Files, 8945-1
2	0899	Technical Library, 4616
1	0612	Review & Approval Desk, 9616 For DOE/OSTI